THE JOURNAL OF PHYSICAL CHEMISTRY A

Article

Assessing the Performance of Dispersionless and Dispersion-accounting Methods: Helium Interaction with Cluster Models of the TiO₂(110) Surface

Maria Pilar de Lara Castells, Hermann Stoll, and Alexander O. Mitrushchenkov

J. Phys. Chem. A, **Just Accepted Manuscript** • DOI: 10.1021/jp412765t • Publication Date (Web): 12 Feb 2014

Assessing the Performance of Dispersionless and Dispersion-accounting Methods: Helium Interaction with Cluster Models of the TiO_2(110) Surface

María Pilar de Lara-Castells *,[1] Hermann Stoll,[2] and Alexander O. Mitrushchenkov[3]

[1]*Instituto de Física Fundamental (C.S.I.C.), Serrano 123, E-28006, Madrid, Spain*

[2]*Institut für Theoretische Chemie, Universität Stuttgart, D-70550 Stuttgart, Germany*

[3]*Université Paris-Est, Laboratoire Modélisation et Simulation Multi Echelle, MSME UMR 8208 CNRS, 5 bd Descartes, 77454 Marne-la-Vallée, France*

(Dated: February 12, 2014)

* E-mail: Pilar.deLara.Castells@csic.es

Abstract

As a prototypical dispersion-dominated physisorption problem, we analyze here the performance of dispersionless and dispersion-accounting methodologies on the helium interaction with cluster models of the TiO_2(110) surface. A special focus has been given to the dispersionless density functional dlDF and the dlDF+D_{as} construction for the total interaction energy (K. Pernal, R. Podeswa, K. Patkowski, and K. Szalewicz, *Phys. Rev. Lett.* **109** (2009) 263201), where D_{as} is an effective inter-atomic pairwise functional form for the dispersion. Likewise, the performance of Symmetry-Adapted Perturbation Theory (SAPT) method is evaluated, where the interacting monomers are described by density functional theory (DFT) with the dlDF, PBE, and PBE0 functionals. Our benchmarks include CCSD(T)-F12b calculations and comparative analysis on the nuclear bound states supported by the He–cluster potentials. Moreover, intra- and inter-monomer correlation contributions to the physisorption interaction are analyzed through the method of increments (H. Stoll, *J. Chem. Phys.* **97** (1992) 8449) at CCSD(T) level of theory. This method is further applied in conjunction with a partitioning of the Hartree-Fock interaction energy to estimate individual interaction energy components, comparing them with those obtained using the different SAPT(DFT) approaches. The cluster size evolution of dispersionless and dispersion-accounting energy components is then discussed, revealing the reduced role of the dispersionless interaction and intra-monomer correlation when the extended nature of the surface is better accounted for. On the contrary, both post-Hartree-Fock and SAPT(DFT) results clearly demonstrate the high transferability character of the effective pairwise dispersion interaction whatever the cluster model is. Our contribution also illustrates how the method of increments can be used as a valuable tool not only to achieve the accuracy of CCSD(T) calculations using large cluster models, but also to evaluate the performance of SAPT(DFT) methods for the physically well-defined contributions to the total interaction energy. Overall, our work indicates the excellent performance of a dlDF+D_{as} approach in which the parameters of the dispersion function are optimized using the smallest cluster model of the target surface. It also paves the way for further assessments of the dlDF+D_{as} approach including periodic boundary conditions as a cost-efficient and accurate method to treat van der Waals adsorbate-surface interactions.

Keywords: Symmetry-Adapted Perturbation-Theory; Post-Hartree-Fock Method of Increments; Helium-Surface Potential; Dispersionless Density-Functional-Theory; var der Waals Adsorbate-Surface Interactions; Titanium Dioxide

I. INTRODUCTION

Nowadays, the first-principle determination of He-surface interaction potentials is a subject of growing interest. This is partly due to the development of low energy helium atom diffraction[1] as an experimental technique to probe surface structure with high resolution, without being perturbed from surface charging and damaging problems. The interest on the He-surface interaction problem has been renewed after the appearance of the helium droplet mediated deposition technique as an experimental tool for the cold attachment of embedded molecules and clusters on surfaces.[2] The microscopic understanding of this process requires quantum dynamical simulations,[3] using realistic He-surface interaction potentials. Last but not least, the physisorption of a helium atom on a surface represents an ultimate case of dispersion-dominated van der Waals (vdW) adsorbate-surface interaction, making it a good test to address more general problems in surface science where vdW interactions play a significant role. Both as a technological relevant surface[4–6] and a prototype transition metal-oxide substrate with well-characterized properties,[4] we have chosen the perfect rutile TiO_2(110)-(1×1) surface.[3,7]

Naturally, cost-efficient calculations of He-surface interaction potentials should use standard periodic electronic structure codes (*e.g.*, `CRYSTAL`[8] and `VASP`[9]), in which methods based on density functional theory (DFT), and Hartree-Fock (HF) or hybrid HF/DFT approaches are implemented using either localized atom-centered Gaussian-type orbitals or plane-wave-based one-electron basis sets. Since these methods are not appropriate to describe the long-range correlation effects in weakly bound systems, the inclusion of long-range dispersive corrections (referred to as +D corrections) has become one of the current standards in DFT-based calculations when physisorption problems are addressed (for e recent review, see Ref. 10). Early attempts to correct the asymptotic behavior of DFT-based approaches when applied to weakly bound complexes date back to the mid-nineties.[11,12] Thus, DFT+D schemes that include semiempirical functions of inter-atomic distances and higher order terms for the dispersion energy, were first proposed by Gianturco and collaborators,[11] and more recently, by Wu and Yang,[13] and by Grimme and collaborators (*e.g.*, the DFT-D2[14] and DFT-D3[15] approaches). Another DFT+D strategy consists in adding the density dependent dispersion correction by Steinmann and Corminboeuf,[16] using the non-local correlation (vdW-DF) functional of Langreth and co-workers,[17] or intermolecular perturbation theory

in a localized orbital basis.[18] Also, a corrected DFT method has been recently developed to include vdW C_6/R^6 terms using maximally localized Wannier functions and applied to physisorption problems in metal surfaces (see, *e.g.*, Ref. 19). The choice of the exchange-correlation functional in DFT+D schemes can be crucial to avoid overbinding effects. This way, the application of the localized molecular orbital decomposition analysis (LMO-EDA)[20] by Jordan and collaborators[21] has illustrated how the overestimation of attractive induction energy components with standard DFT-based methods (typically attributed to deficiencies in the exchange functional) can compensate the shortcomings in the dispersion contribution, giving rise to overbinding effects in DFT+D constructions. Early studies of rare gas cluster ions[22,23] demonstrated the major influence of the chosen exchange functional in DFT-based treatments on the ability to get interaction energies in reasonable agreement with higher level *ab initio* methods, enabling at the same time the calculation of multi-dimensional potential energy surfaces for quantum dynamics simulations.[12] In particular, the necessity of including partial or full "exact" single determinant exchange to avoid overbinding effects was clearly emphasized.[22] Aimed to avoid over-corrections of the inter-monomer interactions in DFT+D schemes, the key idea put forward very recently by Pernal et al.[24] (see also Refs. 25–27) consisted in designing a functional (the so-called dlDF functional) which accounts for the dispersionless interaction energy only so that the dispersion corrections can be safely added later. The dlDF functional is a hybrid meta exchange-correlation functional similar to M05-2X by Zhao, Schultz, and Truhlar[28] from which it differs in the number and values of the DFT parameters. These parameters are optimized using a training set of weakly bound dimers to reproduce benchmark dispersionless interaction energies. To the best of our knowledge, the performance of the dlDF approach in a prototypical He-surface interaction problem is evaluated here for the first time.

Another possibility to describe weakly interacting complexes consists in calculating inter-monomer interaction energies through Symmetry-Adapted Perturbation Theory (SAPT).[29,30] It has the advantage of providing a decomposition of the total interaction energy into physical meaningful electrostatic, exchange-repulsion, induction and dispersion contributions. When combined with a DFT description of the monomer properties, these SAPT(DFT) approaches become particularly efficient.[31–33] The SAPT(DFT) method was simultaneously developed by Misquitta and collaborators[32] (see also Ref. 33), computed in the `SAPT` program, and by Hesselmann and Jansen,[31] who implemented the method into

the MOLPRO package.[34] The application of both implementations to weakly bound systems, for which dispersion dominates the attractive interaction energy component, provided interaction energies of similar accuracy to those obtained with the CCSD(T) method but with much better scaling properties with the basis set size (*e.g.*, see, Ref. 35), in particular when the density-fitting versions of the method are applied.[36,37] Very recently, the SAPT(DFT) method has been applied to adsorbate-surface interaction problems.[7,38] In this work, we evaluate the performance of both dlDF and the SAPT(DFT) method using different DFT approaches in dealing with the physisorption interaction of helium with clusters modeling the TiO_2(110) surface.

For molecular systems, the reliability of dispersion-accounting methods such as the dlDF+D approach is ideally evaluated through the benchmarking with coupled-cluster singles, doubles and noniterative triples [CCSD(T)] calculations using large basis sets or extrapolations to the complete basis set limit. The convergence of the CCSD(T) correlation energy contribution with respect to the basis set size can be accelerated when functions depending explicitly on the inter-electronic coordinates are introduced, for example through the frozen-geminal (F12) CCSD(T)-F12x (x = a, b) approaches.[39,40] During the last years, the implementation of the density-fitting approach, has made possible to perform explicitly correlated CCSD(T)-F12 calculations for small molecular systems. Naturally, the application of these methods is still not feasible using fully periodic models of the He-surface extended system. Concerning the physisorption on non-conducting surfaces, reference interaction energies with periodic models can be obtained at local second-order Möller-Plesset (LMP2) level of theory, as implemented in the CRYSCOR code by Pisani et al.,[41] using the reference crystalline HF orbitals that are provided by a periodic Gaussian-type orbitals calculation with the CRYSTAL code.[8] This method has been recently applied to determine the He–MgO(100) potential interaction.[42] Using the projector-augmented-wave method and plane-wave representations, implementations of non-local *canonical* MP2 and coupled-cluster approaches were introduced,[43,44] but no He-surface potentials have been reported yet. Alternatively, a finite cluster *ansatz* can be adopted to include post-HF effects using coupled-cluster approaches on top of the periodic HF calculations, as applied with the method of increments. This method was originally developed by Stoll[45] and successfully applied to account for correlation effects in many extended systems such as diamond,[45], bulk rutile,[46] and carbon-based surfaces.[47] The method of increments has been very recently applied by Paulus

and collaborators[48,49] and Staemmler[50] to adsorption[49] and physisorption problems[50,51] using both hydrogen-terminated clusters[51] and point-charge-based cluster embedding.[49,50]

Aimed to include post-HF effects using embedded cluster models, the "cluster-in-solid" technique[52] was developed and implemented as an interface[53] between the CRYSTAL code and the MOLPRO package of *ab initio* programs.[34] Very recently, this method has been successfully applied to get the correlated band structure of bulk rutile TiO_2.[54] Later on, it was applied to add correlation corrections at CCSD(T) level of theory into the interaction between a helium atom and an embedded cluster modeling the TiO_2(110) surface.[7] Linear-dependence problems in the periodic HF calculations with Gaussian-type orbitals prevented from using the specially diffuse basis set that is necessary to characterize the He-surface interaction. Nonetheless, the similarity between the correlation energies obtained using embedded cluster models with smaller basis sets and the hydrogen-terminated cluster counterparts, indicated the suitability of using hydrogen-saturated clusters to get insights into the physisorption interaction at higher levels of *ab initio* theory.

In this study, hydrogen-saturated cluster models of the TiO_2(110) surface are used for the benchmarking of dispersionless and dispersion-accounting approaches. Previous periodic calculations using the Perdew-Burke-Ernzerhof (PBE) functional[55] and an electronic basis set tailored to minimize the basis set superposition error (BSSE), yield a short and medium-range interaction He-surface potential in very reasonable agreement with LMP2 results obtained with a large cluster of stoichiometry $(TiO_2)_9(H_2O)_{16}$. In contrast, the PBE+D2 scheme produced clear overbinding effects. The first part of this paper is aimed to understand the fundamental reasons of this behavior using the LMO-EDA scheme of Su and Li.[20] More importantly, using a sequence of clusters, this work is aimed to evaluate the performance of both the dlDF+D approach proposed by Pernal et al.[24] and the SAPT(DFT) method[31,32] using different DFT approaches to account for the dispersionless and dispersion components of the interaction. For this purpose, reference interaction energies are obtained through CCSD(T)-F12b, CCSD(T), and LCCSD(T) calculations depending on the cluster size. Our benchmarking is not only performed on interaction energies but also on the nuclear bound states and corresponding vibrational frequencies. Further physical insights into the physisorption interaction and additional benchmarking are achieved by applying the methods of increments at CCSD(T), LCCSD(T), LMP2 and MP2 levels of theory. As will be shown, this method allows to separate the correlation contribution to

the total interaction energy into inter- and intra-monomer parts. When combined with a LMO-EDA-based decomposition of the HF interaction energy, estimates for the electrostatic, exchange-repulsion, induction and dispersion energy components can be obtained and compared with the SAPT(DFT) counterparts, using different density functionals for the monomers. Next, the dispersion energies for a given cluster size are fitted to the dispersion functional form proposed by Podeszwa and Szalewicz[26] (denoted as $D_{\rm as}$), and the dispersion energies directly calculated with the SAPT(DFT) method (hereafter referred to as D) are compared with those extracted with the $D_{\rm as}$ functional using clusters of increasing size. The method of increments is also applied to prove the transferability of the effective pairwise dispersion interactions in expanding the cluster model. Moreover, the combined application of SAPT(DFT) and supermolecular DFT and post-HF methods with LMO-EDA and incremental-based decompositions has allowed us to explain *how and why* the physisorption interaction is modified by the modeling of the rutile surface with clusters of increasing size, with the emphasis on the relative weights of dispersion and dispersionless contributions as well as intra- and inter-monomer correlation effects.

This paper is structured as follows. Section II contains the computational details and a brief outline of the applied methods. In the first part of Section III, the results for the He–$(TiO_2)(H_2O)_3$ complex are presented and discussed, with the main purpose of understanding the characteristics of the interaction and assessing the performance of the applied methodologies. The second part of this section extends the application of SAPT(DFT) and dlDF+D approaches as well as the method of increments to larger clusters modeling the $TiO_2(110)$ surface. Section IV closes with the conclusions.

II. APPLIED METHODS AND COMPUTATIONAL DETAILS

All the electronic structure calculations have been performed with the `MOLPRO` suite of programs.[34] For this purpose, we have implemented the LMO-EDA scheme of Su and Li[20] in the `MOLPRO` package using the `MATROP` facility. To implement the dlDF functional,[24] we modified the parameters of the M05-2X functional.[28] On the other hand, the nuclear bound-state calculations were accomplished using the Truhlar-Numerov procedure,[56] as described below.

A. Cluster models

The hydrogen-saturated clusters chosen to characterize the He–TiO_2(110) interaction are represented in Fig. 1. They are very similar to those used by Rittner at al.[57] to model the N_2–TiO_2(110) system. We consider the He-cluster interaction as a function of the vertical height z above the most stable adsorption site (the five-coordinated Ti(5f) atom), with a z grid in the range [2.8–10.0] Å. As already mentioned in Ref. 7, the number of hydrogen atoms was chosen to make the clusters electrically neutral, adding them along the O–Ti direction in the extended system. As in Ref. 7, we define the main interaction region as that formed by the Ti(5f) adsorption site and their nearest in plane surface and bridging oxygen atoms (denoted as O_p and O_b in Fig. 1). The geometry of the clusters has been frozen to the experimental geometry of the TiO_2(110)–(1×1) surface.[58] This approach is justified by the fact that only minor surface ion displacements upon helium physisorption were observed (0.0013 Å as much).[3] The cluster of stoichiometry $(TiO_2)(H_2O)_3$ (denoted as $\mathcal{C}_1$, see Fig. 1) has served to characterize the interaction of the helium atom with the Ti(5f) adsorption site and its nearest (in-plane and sub-surface) oxygen neighbors from the TiO_2(110) surface. The relatively small size of this cluster has allowed us to perform all-electron explicitly correlated CCSD(T)-F12b calculations for benchmarking purposes. The next cluster model (the $\mathcal{C}_2$ cluster with stoichiometry $(TiO_2)_3(H_2O)_5$, see Fig. 1) is obtained by extending the $\mathcal{C}_1$ cluster along the Ti(5f) row (i.e., the crystallographic [001] direction). This way, our analysis is extended to the physisorption interaction of helium with the two next-nearest Ti(5f) atoms and their respective coordination shells of oxygen atoms. The largest cluster of stoichiometry $(TiO_2)_9(H_2O)_7$ (the $\mathcal{C}_3$ cluster, see Fig. 1) has enabled to characterize the role of the bridging oxygen atoms sticking out of the surface[7]. It involves the expansion of the $\mathcal{C}_2$ cluster along the crystallographic [$\bar{1}$00] direction. As shown in Fig. 1, the $\mathcal{C}_1$ and $\mathcal{C}_2$ clusters model the top molecular layer only while the largest $\mathcal{C}_3$ cluster partially accounts for the interaction with atoms from the first under-surface molecular layer.

B. Supermolecular calculations

Using the supermolecular approach, the interaction energy between a single helium atom and the cluster modeling the $TiO_2(110)$ surface $\mathcal{C}(TiO_2)$ is expressed as,

$$E_{\rm int}^{\rm tot} = E_{\rm He-\mathcal{C}(TiO_2)} - E_{\rm He} - E_{\mathcal{C}(TiO_2)}, \tag{1}$$

where $E_{\rm He-\mathcal{C}(TiO_2)}$ is the total energy of the He–$\mathcal{C}(TiO_2)$ complex, and $E_{\rm He}$ and $E_{\mathcal{C}(TiO_2)}$ are the energies of the monomers. We used the counterpoise procedure proposed by Boys and Bernardi[59] to account for the intra-molecular basis set superposition error (BSSE). To estimate the dispersionless contribution to the total interaction energy, we have used the dlDF functional developed by Szalewicz and collaborators.[24] The parameters of the M05-2X functional[28] as present in `MOLPRO` were modified to implement the dlDF functional. This allowed us to calculate dlDF interaction energies and to perform SAPT(dlDF) calculations. The implementation was tested by reproducing the same dlDF interaction energies presented as a training set data in Ref. 24.

Using wave-function-based post-Hartree-Fock methods, $E_{\rm int}^{\rm tot}$ is partitioned as,

$$E_{\rm int}^{\rm tot} = E_{\rm int}^{\rm HF} + E_{\rm int}^{\rm corr} \tag{2}$$

where $E_{\rm int}^{\rm HF}$ and $E_{\rm int}^{\rm corr}$ represent the Hartree-Fock and correlation contributions to the total interaction energies. Along with standard correlation methods, the term $E_{\rm int}^{\rm corr}$ has been calculated with the method of local increments.[45] Detailed descriptions of this method can be found in Refs. 47,60,61 and, as applied to adsorption energies, in Refs. 50,51. In this method, the correlation energy $E^{\rm corr}$ is first expressed as a cumulant expansion of contributions (increments) from groups of occupied localized orbitals on different atoms (or group of atoms),[46]

$$E^{\rm corr} = \sum_A \epsilon(A) + \sum_{A<B} \Delta\epsilon(A-B) + \sum_{A<B<C} \Delta\epsilon(A-B-C), \tag{3}$$

where A, B, C, $\cdots$ denote localized orbital groups on atoms (or atomic groups) indexed by A, B, C, $\cdots$, respectively. The one-body term ϵ_A represents the correlation energy obtained when the electrons from the localized orbital group A are correlated, freezing the rest of localized orbitals. The two-body increment is defined as the non-additive part of the correlation energy associated to the simultaneous correlation of the electrons from the

localized orbital groups A and B:

$$\Delta\epsilon(A-B) = \epsilon(A-B) - \epsilon(A) - \epsilon(B). \tag{4}$$

Similarly, the three-body increments $\Delta\epsilon(A-B-C)$ is calculated by subtracting the one- and two-body energy increments involving the orbital groups A, B and C from the energy obtained upon the simultaneous correlation of the electrons occupying the same localized orbitals (see, *e.g.*, Ref. 46).

To obtain the correlation contribution to the interaction energy $E_{\rm int}^{\rm corr}$, it is necessary to calculate the increment modifications due to the interaction between the monomers, including all the orbital groups from the cluster $\mathcal{C}(\mathrm{TiO_2})$ modeling the $\mathrm{TiO_2}(110)$ surface that are interacting with the helium atom. In this particular case, the most important orbital groups of the surface would be the occupied localized orbitals generated from the $2s$ and $2p$ atomic orbitals centered at the oxygen atoms in the vicinity of the adsorbed species. Using a similar notation to that of Ref. 51, the one-body increment contribution to $E_{\rm int}^{\rm corr}$ from the group of localized orbitals centered on the ith oxygen atom of the $\mathcal{C}(\mathrm{TiO_2})$ cluster can be written as,

$$\eta(\mathrm{O}^{(i)}) = \epsilon^{\mathrm{He}-\mathcal{C}(\mathrm{TiO_2})}(\mathrm{O}^{(i)}) - \epsilon^{\mathcal{C}(\mathrm{TiO_2})}(\mathrm{O}^{(i)}). \tag{5}$$

Similarly, the two-body increment contribution to $E_{\rm int}^{\rm corr}$ arising from the groups centered on the ith and jth oxygen atoms is calculated as,

$$\eta(\mathrm{O}^{(i)}-\mathrm{O}^{(j)}) = \Delta\epsilon^{\mathrm{He}-\mathcal{C}(\mathrm{TiO_2})}(\mathrm{O}^{(i)}-\mathrm{O}^{(j)}) - \Delta\epsilon^{\mathcal{C}(\mathrm{TiO_2})}(\mathrm{O}^{(i)}-\mathrm{O}^{(j)}). \tag{6}$$

When the increments involve groups of both the surface and the adsorbate, $\eta(A-B)$ and $\Delta\epsilon(A-B)$ share the same definition. Therefore, $E_{\rm int}^{\rm corr}$ can be expanded as,

$$E_{\rm int}^{\rm corr} = \eta(\mathrm{He}) + \sum_i \eta(\mathrm{O}^{(i)}) + \sum_i \eta(\mathrm{He}-\mathrm{O}^{(i)}) + \sum_{i<j} \eta(\mathrm{O}^{(i)}-\mathrm{O}^{(j)}) + \sum_{i<j} \eta(\mathrm{He}-\mathrm{O}^{(i)}-\mathrm{O}^{(j)}) + \cdots$$

It should be noticed that all the increments are calculated using the full basis set so that $E_{\rm int}^{\rm corr}$ becomes counterpoise corrected. Along with the incremental scheme, benchmark calculations have been performed using the CCSD(T)-F12b method for the He–$\mathrm{C_1}$ complex, as discussed below. In both cases, the semi-core $3sp$ orbital from the Ti atom were kept frozen and not correlated.

C. Calculations using Symmetry-Adapted Perturbation Theory

In this work, the SAPT method has been used with a DFT description of the helium atom and the cluster modeling the rutile surface, as implemented in the DFT-SAPT code.[31,36] We will refer this method as SAPT(DFT), replacing DFT by the functional name when a particular functional is considered. An independent implementation of this method by Misquitta et al. has been also reported.[33] This method enables to calculate the interaction energy as a sum of individual first- and second-order interaction terms, namely electrostatic $E^{(1)}_{elst}$, exchange $E^{(1)}_{exch}$ induction $E^{(2)}_{ind}$, and dispersion $E^{(2)}_{disp}$ terms, along with their respective exchange corrections ($E^{(2)}_{exch-ind}$ and $E^{(2)}_{exch-disp}$). The δ(HF) estimate[36,62] of the higher-order induction plus exchange-induction contributions has been added to the DFT-SAPT interaction energy. The density-fitting (DF) technique has been used to calculate SAPT(DFT) interaction energies of the He–$\mathcal{C}_2$ and He–$\mathcal{C}_3$ complexes (see Fig. 1), as implemented within `MOLPRO` by Hesselmann, Jansen and Schütz.[36] No DF was employed for the SAPT(DFT) calculations of the He–$\mathcal{C}_1$ complex. Molecular orbitals for SAPT(DFT) were obtained from Kohn-Sham (KS) calculations using the PBE,[55] PBE0,[63] and dlDF[24] functionals.

In all calculations, the exchange-correlation (xc) potentials were asymptotically corrected following the gradient-regulated scheme of Grüning *et al.*[64]. As described in Ref. 64, this correction to the exchange-correlation (xc) potential was devised to enforce the right long-range behaviour (i.e., decaying as $-1/r$), shifting at the same time the highest occupied molecular orbital (HOMO) energy ϵ_{HOMO} to the ionization potential (IP) value I_p (i.e., satisfying the condition $\epsilon_{\mathrm{HOMO}} = -I_p$). To achieve this goal[64], the potential is shifted by $I_p + \epsilon_{\mathrm{HOMO}}$. The eigenvalues of the KS orbitals (in particular the unoccupied orbitals) supported by exchange-correlation (xc) potentials with wrong asymptotic decay are usually too high, as occurs with the HOMO eigenvalue. The inaccuracies in the KS eigenvalue spectra (e.g., the differences between the occupied and unoccupied energies) are naturally reflected in the response functions employed to determine the induction and dispersion energies. The HOMO eigenvalues of the monomers have also a pronounced influence on the exchange-repulsion component (for details see Ref. 65). Likewise, asymptotically corrected xc potential are necessary to get accurate tails of the monomer densities, and then of the charge overlaps entering into the electrostatic energy determination[65]. This way, it has been shown[33,65] that the inclusion of the asymptotic correction in SAPT(DFT) calculations

improve much the interaction energies, making them less dependent on the density functional used. We employed ionization potential (IP) values of 0.9036 and 0.3491 a.u. for atomic He and the fragment modeling the rutile surface, respectively, and the HOMO energies (resulting from the corresponding standard DFT calculations on the monomers) to calculate the shift parameter $I_p + \epsilon_{\mathrm{HOMO}}$. The IP values are those reported in the NIST Chemistry Web Book[66] for atomic helium and (gas-phase) TiO_2. Another alternative would have been to use either the TiO_2(110) surface work-function (0.2021 a.u. from Ref. 67) or the Koopmans' theorem IP values from HF computations at each cluster size as in Ref. 38. However, a very similar IP value (0.3409 a.u.) to the TiO_2 gas-phase value was obtained for the $\mathcal{C}_1$ cluster at CCSD(T) level while the HF counterpart was about 0.08 a.u. too high. On the other hand, the Hartree-Fock IP value varied very little in going from the $\mathcal{C}_1$ to the $\mathcal{C}_3$ cluster (to within 7%) and a similar trend can be expected for the correlated IP counterpart. We have also tested that the employment of the TiO_2(110) work-funcion as the IP value for the SAPT(DFT) calculations on the He$-\mathcal{C}_3$ complex make the interaction energies about 15% less attractive and worsen the agreement with the best benchmarking.

The adiabatic local density approximation (ALDA)[68] has been used in all SAPT(PBE) calculations. Since the PBE0 and dlDF exchange potentials contain 25% and 61.44% of single-determinant exchange, a hybrid-ALDA kernel with the same percentage of Fock exchange has been employed to get both the static and frequency-dependent response functions in SAPT(PBE0) and SAPT(dlDF) calculations for the He–$\mathcal{C}_1$ complex. However, the current density-fitting implementation of the SAPT(DFT) method within `MOLPRO` can only deal with pure ALDA kernels in computing the response functions. Therefore, this approximation is also used in SAPT(DFT) calculations with hybrid functionals to calculate the dispersion energy component for the He–$\mathcal{C}_2$ and He–$\mathcal{C}_3$ complexes. To stress the use of a pure ALDA kernel in conjunction with the hybrid PBE0 and dlDF functionals in the dispersion energies, the SAPT calculations will be referred to as SAPT(ALDA/PBE0) and SAPT(ALDA/dlDF), respectively.

D. Localized molecular orbital energy decomposition analysis

The localized molecular orbital energy decomposition analysis (LMO-EDA) of Su and Li[20] has been used to separate the total interaction energy obtained from supermolecular HF and

PBE calculations into electrostatic, exchange-repulsion (or exchange), induction, and inter-monomer correlation contributions, comparing them to those obtained from SAPT-based calculations. This scheme has been implemented in the MOLPRO package through the MATROP module. The electrostatic and exchange contributions are calculated by freezing the occupied monomer molecular orbitals. The former is defined as the Coulomb interaction between the electrons and nuclei of the two monomers and the explicit expression is equivalent to that implemented for the SAPT $\mathrm{E}^{(1)}_{elst}$ component (Eq. (2) of Ref. 36). Using the LMO-EDA partitioning in DFT, the exchange contribution is defined as,

$$\mathrm{E}_{exch} = E_x[\rho_{\mathrm{He}} + \rho_{\mathcal{C}(\mathrm{TiO_2})}] - \{E_x[\rho_{\mathrm{He}}] + E_x[\rho_{\mathcal{C}(\mathrm{TiO_2})}]\}, \tag{7}$$

where ρ_{He} and $\rho_{\mathcal{C}(TiO_2)}$ denote KS densities of the helium atom and the cluster modeling the rutile surface, respectively. On the other hand, the calculation of the repulsion contribution requires the mutual orthogonalization of the occupied monomer molecular orbitals. This contribution is defined as the difference between the KS energy (excluding the correlation term) obtained with the first-order reduced density matrices calculated with the orthogonalized molecular orbitals, and the counterpart using the original molecular orbitals. For example, the exchange contribution to the repulsion term (E^{exch}_{rep}) is given as,

$$\mathrm{E}^{exch}_{rep} = E_x[\rho^{ortho}_{\mathrm{He}} + \rho^{ortho}_{\mathcal{C}(\mathrm{TiO_2})}] - E_x[\rho_{\mathrm{He}} + \rho_{\mathcal{C}(\mathrm{TiO_2})}], \tag{8}$$

where the subscript "ortho" indicates that the densities have been obtained after orthogonalizing the monomer molecular orbitals. Besides the changes in the electrostatic terms, the repulsion contribution also accounts for the modification in the one-particle kinetic energies due to the orthogonalization procedure.

Using the LMO-EDA scheme, the KS orbital relaxations due to the inter-monomer interaction itself are accounted for within the induction and inter-monomer correlation contributions, with the latter expressed as,

$$\mathrm{E}^{\mathrm{inter}}_{corr} = E_c[\rho_{\mathrm{He}+\mathcal{C}(\mathrm{TiO_2})}] - \{E_c[\rho_{\mathrm{He}}] + E_c[\rho_{\mathcal{C}(\mathrm{TiO_2})}]\}, \tag{9}$$

where ρ_{He} and $\rho_{\mathcal{C}(TiO_2)}$ denote KS densities of the helium atom and the cluster modeling the rutile surface, respectively, and $\rho_{\mathrm{He}+\mathcal{C}(\mathrm{TiO_2})}$ is the electron density minimizing the He–$\mathcal{C}(\mathrm{TiO_2})$ KS energy. This correlation contribution has been identified with the short-range contribution to the dispersion energy,[20,21] adopting the same interpretation here. In comparing the

LMO-EDA and SAPT(DFT) results, the dispersion and exchange-dispersion SAPT(DFT) contributions were combined as were the induction, exchange-induction and δ(HF) contributions. Similarly, the exchange and repulsion LMO-EDA terms were added to calculate the net exchange-repulsion energy contribution.

E. Electronic Basis Sets and Orbital Localization

1. Basis Sets in DFT, LCCSD(T), and SAPT(DFT) Calculations

Unless otherwise specified, supermolecular DFT/LCCSD(T) and SAPT(DFT) calculations were performed using an augmented triple-ζ valence all-electron basis set[69] for O and Ti atoms (the so-termed ext-TVAE** basis[7]). This is a dual basis that includes additional diffuse functions for the O and Ti atoms within the main interaction region (see Ref. 7 for the details). Both helium and hydrogen atoms were described with the standard aug-cc-pVTZ basis set of Dunning and collaborators.[70,71] The density fitting technique was used in both dlDF and SAPT-based calculations on the He–$\mathcal{C}_2$ and He–$\mathcal{C}_3$ complexes, as implemented within MOLPRO.[36,72] The DF of Coulomb and exchange J/K integrals has used the auxiliary basis set developed for the cc-pVTZ basis by Weigend,[73] while the aug-cc-VTZ/MP2Fit basis[74] was employed to fit the integrals containing virtual orbitals. The suitability of both the ext-TVAE** basis and the density fitting approximation was tested for either DFT or SAPT(DFT) calculations as follows:

- Using the additional diffuse functions of the ext-TVAE** basis for all the atoms composing the $\mathcal{C}_2$ cluster, the He–$\mathcal{C}_2$ interaction energies deviated from those obtained with the dual basis by less than 2%. Similarly, dispersionless and dispersion SAPT(DFT) interaction energies agreed with those calculated with the dual basis to within 1% and 4%, respectively. On the other hand, the omission of these functions for the atoms within the main interaction region resulted in interaction energy differences amounting to about 6% and 15% in dlDF and SAPT(dlDF) calculations, respectively.

- The error in dlDF interaction energies due to the density-fitting was below 0.1 cm^{-1} for the He–$\mathcal{C}_2$ complex at the vdW minimum, with the relative error being below 1% at the relevant range of inter-monomers He–Ti(5f) distances. Similar errors were found in the SAPT(DFT) energy components upon the density-fitting approximation with the

exception of the dispersion terms when hybrid DFT functionals are used (see Section III).

2. Basis Sets in Explicitly Correlated Coupled-Cluster Calculations

Following an accurate study of transition-metal containing molecules, explicitly correlated CCSD(T) calculations were performed using the CCSD(T)-F12b method[40], with the cc-pVnZ-F12 (n=T, Q) series of orbital basis sets for H, He and O[75] and the aug-cc-pVnZ (n=T, Q) basis of Dunning and collaborators[70,71] for Ti. These orbital basis sets will be termed AVTZ and AVQZ for n =T and Q, respectively. Density-fitting within the correlation treatment used the aug-cc-pVnZ/MP2Fit[74] (n=T, Q) auxiliary basis sets for H, He and O atoms, respectively. The Fock matrix fitting was carried out with the def2-QZVPP/JKFit[76] auxiliary basis sets for Ti and He atoms, and the cc-pVnZ/JKFit (n=T, Q) sets for the other elements. The complementary auxiliary basis approach[77] for the resolution of the identity employed the OptRI auxiliary basis sets matching to the corresponding orbital basis sets.[78–80] The DF/MP2Fit fitting basis was used along with the complementary auxiliary basis optimized for the aug-cc-pVnZ (n=T, Q) sets centered on the Ti atom (see Ref. 81). As in previous studies of transition-metal containing systems,[80,82] the value of the geminal Slater exponent was fixed to 1.4 a_0^{-1}.

We extrapolated the CCSD(T)-F12b correlation energies to the complete basis set limit (CBS) by applying the scheme proposed by Helgaker and co-workers[83] for standard CCSD(T) calculations,

$$E_n^{corr} = E_{\rm CBS}^{corr} + A\ \ell_{\rm max}^{-3} \tag{10}$$

where the angular quantum number ℓ_{max} is simply settled to the n cardinal number in the AVnZ (n =T, Q) basis set. The HF interaction energies were fixed to those obtained with the largest basis. When applied to very weak interacting dimers with explicitly correlated coupled-cluster methods, an extensive analysis by Patkowski[84] has shown that the $1/n^3$ scheme provides reliable estimations of the CBS limit. Different extrapolation schemes were tested (see, *e.g.*, Ref. 85), providing very similar values. It should be noticed that basis set extrapolation schemes specially designed for F12 methods have been developed[86] but not yet reported for transition-metal containing systems. In any case, the CCSD(T)-F12b interaction energies with the AVQZ basis were found to be very close to the estimated CBS

limit (see Section III).

3. Basis sets and Localization in Calculations with the Method of Increments

The method of increments has been applied to the He–$(TiO_2)(H_2O)_3$ complex by using the polarized correlation-consistent valence-triple-ζ basis (cc-pVTZ) of Dunning and collaborators[70,71] for Ti and H, and the aug-cc-pVTZ basis for He and O (to be denoted as (A)VTZ). As in the CCSD(T)-F12b/AVQZ calculations, only the valence electrons were correlated. For the incremental expansion, the occupied valence orbital space was partitioned into six orbital groups that can be attributed to the helium atom and individual (Ti–)O_pH or (Ti–)$O_{sub}H_2$ groups from the $\mathcal{C}_1$ cluster model (see Fig. 1). The Foster-Boys localization procedure[87] was employed, as implemented in MOLPRO.[34] Each (Ti–)O_bH [(Ti–)$O_{sub}H_2$] atomic group consists of four double occupied orbitals. They are mainly composed of the $2s$ and $2p$ atomic orbitals centered at the surface in-plane oxygen anions O_p (the sub-surface oxygen atom O_{sub}). Clearly, titanium atoms also participate in the orbital groups, which is manifested through the hybridization (mainly with Ti($3d$) atomic orbitals) during the Foster-Boys localization. Obviously, the adsorbate species subunit consists of a double occupied localized orbital, as generated from the atomic orbital $1s$ centered at the helium atom. The incremental expansion was truncated after the most important three-body terms. The suitability of this setup was evaluated by comparing the correlation contributions from the incremental expansion ($-73.128/-47.598$ cm^{-1} at $z = 3.5/3.875$ Å, respectively) to those obtained from full CCSD(T) calculations ($-72.774/-47.316$ cm^{-1}), agreeing to within 0.5%.

The incremental scheme has been also applied to the He–$(TiO_2)_9(H_2O)_7$ complex by calculating the most important correlation contributions to the interaction energy. In this case, the increments were calculated at MP2, LMP2, LCCSD(T), and CCSD(T) levels of theory. As for the He–$(TiO_2)(H_2O)_3$ dimer, only the valence electrons were correlated and the counterpoise correction was included. We used the cc-pVDZ basis for H and Ti, and the aug-cc-pVDZ basis for O and He. For the atoms outside the main interaction region[7], the polarization functions were omitted. For the He–$(TiO_2)(H_2O)_3$ dimer, the omission of these functions resulted in differences for the main correlation contributions to within 1–4%. Hereafter, this basis will be referred to as (A)VDZ.

F. Calculation of Nuclear Bound States

To calculate the bound states supported by the He–$(TiO_2)(H_2O)_3$ potential energy curve (PEC), the interaction energies were first fitted to a Morse functional form with a damped long-range $-f(z;z_0,a)\left(\frac{C_3}{z^3}\right)$ term, where,

$$f(z;z_0,a) = \frac{1}{2}\left\{1+\tanh\left[\frac{z-z_0}{a}\right]\right\}. \quad (11)$$

Next, the energies and nuclear wave-functions were calculated by numerically solving the one-dimensional Schrödinger equation through the Truhlar-Numerov procedure,[56] using a numerical grid of 100000 points in the range [1.0–1000.0] a.u. The atomic masses were fixed to the following values (in amu): m_{Ti}=46.8671, m_O=15.9994, m_H=1.00794, and $m_{^4He}$=4.002602.

III. RESULTS AND DISCUSSION

The results are organized as follows: The different clusters modeling the rutile surface are shown in Fig. 1. Using the smallest cluster model of stoichiometry $(TiO_2)(H_2O)_3$ (referred to as $\mathcal{C}_1$), Figures 2 and 4 provide the He–cluster interaction energies as a function of the inter-monomer distance. For the sake of clarity, Table I collects the magnitudes characterizing these potential energy curves. Next, the individual components of the interaction at the vdW minimum are schematically represented in Fig. 3. The interaction is further analyzed using correlation increment contributions, which are collected in Table II. Additional benchmarking is obtained by calculating the nuclear bound states supported by the He–$\mathcal{C}_1$ potential energy curves, with the leading vibrational energies and density distributions shown in Table III and Fig. 5, respectively.

The second part of this section extends our study to the larger cluster models of stoichiometries $(TiO_2)_3(H_2O)_5$ and $(TiO_2)_9(H_2O)_7$ (denoted as $\mathcal{C}_2$ and $\mathcal{C}_3$, respectively). The potential energies curves of the He–$\mathcal{C}_2$ and He–$\mathcal{C}_3$ complexes are represented in Figs. 6 and 9, while the cluster size evolution of the individual interaction energy components, as calculated with the SAPT(DFT) method, can be followed from Fig. 7. The method of increments has been also applied to the He–$\mathcal{C}_3$ system with the main correlation contributions summarized in Table IV. Finally, the cluster size evolution of dispersionless and dispersion interaction energies depending on the chosen DFT method (within the SAPT(DFT) framework) is graphically represented in Figure 8.

A. The He–$(TiO_2)(H_2O)_3$ complex: performance of DFT+D approaches

As already mentioned, Figure 2 shows He–$(TiO_2)(H_2O)_3$ interaction energies as a function of the distance between the helium atom and the Ti(5f) cation, using the different methods considered in this work (see also Table I). Focusing first on the PECs obtained with the PBE and PBE+D2 approaches, it can be immediately noticed that the PBE functional provides a very reasonable short- and medium-range potential energy curve, in contrast with the PBE+D2 scheme. Thus, the PBE well-depth and minimum energy positions are very close to those obtained in the conventional CCSD(T)/(A)VTZ calculations. Naturally, due to the inability of the semi-local PBE functional to account for long-range dispersion, the attractive tail of the potential is not described correctly, which is also reflected in the discrepancy between PBE and CCSD(T)/(A)VTZ zero-point energies. The inclusion of the empirical dispersion correction with the Grimme's D2 scheme[14] improves the asymptotic region (at distances larger than $\sim$ 5.0 Å). However, it also causes a very pronounced overbinding effect, with the well-depth being a factor of $\sim$ 2.4 larger than the CCSD(T)-F12b/AVQZ value. Many previous studies have shown that the PBE+D2 scheme works reasonably well in extended systems where the vdW interaction plays a key role (*e.g.*, soft layered materials[88] or water physisorption[51] to name just two). In order to understand the fundamental reasons for the good performance of the PBE approach at the vdW minimum (and the consequent poor behavior of the PBE+D2 construction), we have decomposed the net PBE interaction energy using the LMO-EDA scheme developed by Su and Li[20] (see Section II). The results are shown in Fig. 3 along with those obtained through SAPT(DFT) calculations and the LMO-EDA-based decomposition of the HF interaction energy, with and without adding the correlation contributions extracted from supermolecular CCSD(T)/(A)VTZ calculations with the method of increments, as described below.

As clearly apparent form Fig. 3 (notice the small magnitudes of the electrostatic and induction contributions), the weak physisorption interaction results from the balance of the short-range exchange-repulsion and the attractive long-range dispersion energy term, with the latter dominating at the vdW minimum and at larger inter-monomer distances. Of course, the dispersion energy arises from a pure electron correlation effect so that the HF interaction is repulsive. Adding the exchange-repulsion and dispersion-like contributions to E_{int}^{tot} from CCSD(T) calculations with the method of increments, we get an attractive

interaction of similar magnitude to that obtained with the SAPT(PBE0) approach. The individual $E_{exch-rep}$ and E_{disp} contributions also agree very well to each other, which is remarkable. From Figure 3, it can be also noticed that the exchange-repulsion is enhanced when the correlation obtained with the CCSD(T) method is accounted for. Contrarily, when the correlation is estimated through the PBE approach, the exchange-repulsion component has a very similar magnitude to the uncorrelated HF counterpart. As apparent from Figure 3, the good performance of the PBE approach can be attributed to both the recovering of some part of the short-range dispersion through the inter-monomer correlation contribution, as identified within the LMO-EDA framework[21] (see Eq. 9), and to a cancellation of errors: this functional underestimates the exchange-repulsion LMO-EDA energy, and overestimates the attractive induction contribution, partially compensating for the underestimation of the dispersion component. It follows that the inclusion of an additional attractive dispersion term through the DFT-D2 scheme overcorrects the interaction.

The tendency of DFT methods to overestimate the induction contribution in weakly bound systems such as water clusters has been noticed previously[21] and attributed to the self-interaction error in DFT.[89] In contrast to the LMO-EDA of water clusters, however, the overestimation of the induction He–$(TiO_2)(H_2O)_3$ interaction with the PBE approach is not accompanied by that of the exchange-repulsion. This could explain one of the reasons why dispersion-corrected PBE+D approaches work better in water clusters. The larger value of the electrostatic term with the PBE approach (see Fig. 3) reflects the strongest overlap between the monomer densities. Hence, a larger magnitude for the exchange-repulsion would be expected, as opposed to the results shown in Fig. 3. This feature can be attributed to the exchange functional. This way, the replacement of the PBE exchange functional by the revPBE variant[90] (which differs by a single parameter to mimic the short-range Hartree-Fock behavior) modifies the exchange energy to such extent that the net revPBE exchange-repulsion becomes the largest between those shown in Fig. 3. The same holds true when the PBE exchange is replaced by the single-determinant counterpart (i.e., from the KS Fock operator).

As mentioned in the introduction, the dlDF functional of Pernal et al.[24] was designed to account for the dispersionless interaction energy only, avoiding over-corrections in DFT+D constructions. Consequently, as apparent from Fig. 2, the dlDF functional provides a purely repulsive PEC for the He–$(TiO_2)(H_2O)_3$ interaction and, once the dispersion is accounted for

(leading to the dlDF+D approach, see Fig. 2), we obtain a PEC in very reasonable agreement with the benchmark obtained using the CCSD(T)-F12b method (see also Table I). Since the parameters entering the dlDF functional were not optimized with a training set containing transition-metal atoms, the good performance of the dlDF approach is remarkable.

B. The He–$(TiO_2)(H_2O)_3$ complex: analysis of the interaction with the method of increments

Let us now analyze the He–cluster interaction from a local viewpoint. This is possible by applying the method of increments, which can distinguish the correlation contributions coming from different cluster regions. Moreover, this method allows to separate between intra- and inter-monomer correlation effects. Selected correlation-energy contributions to the total interaction energy are collected in Table II. Focusing first on the increment contributions at $z = 3.5$ Å, by far the largest contribution comes from the two-body interaction of the helium atom with the adjacent O_p atoms located at the surface plane (see Fig. 1). The increments involving the subsurface oxygen atoms that beneath the Ti(5f) adsorption site are very small, only amounting to 6% of the total correlation energy contribution. The total attractive contribution is overshooted by about 30%. The most important reduction comes from the one-body increments of the adjacent O_p atoms (or rather their modification with respect to those calculated for the bare $(TiO_2)(H_2O)_3$ cluster). The contributions from the three-body interaction between the helium atom and two surface O_p atoms (and the corresponding modifications of these surface O_p two-body increments with respect to the bare $(TiO_2)(H_2O)_3$ cluster) equal to 6% of the two-body counterparts.

As discussed in Refs. 50,51, the two-body and three-body inter-monomer increments can be interpreted as two-body and three-body dispersion-like terms. This interpretation is further supported by the excellent agreement of the net dispersion energies with those calculated through the SAPT(DFT) method (see Fig. 3 and the bottom panel of Fig. 4). Indeed, the correlation part coming from the interaction of He and surface oxygen atoms (O_p) fits to better than 0.15 cm^{-1} (3%) to a $-C_6/R^6 - C_8/R^8$ functional form over the considered range of He–O_p distances (from 3.3 to 5.4 Å). The root-mean-square (RMS) of residuals (0.21 cm^{-1}) increased by a factor of 7 if the R^{-8} term is omitted in the fitting, with the C_6 coefficient raising from 8.737 to 15.158 a.u. These values are around the one calculated

with the Slater-Kirkwood formula for the interaction of a Helium atom O^{2-} anion (11.470 a.u from Ref. 3). As already mentioned, however, it should be taken into account that the valence Ti($3d$) orbitals also participate in the localized orbitals groups centered on the O_p atoms. To estimate C_6 coefficients for the He–Ti^{4+} interaction, we would need to correlate the semicore Ti($3sp$) orbitals. Due to the small Ti^{4+} static polarizability (more than an order of magnitude smaller than for the O^{2-} anion,[91]) the associated two-body increments are expected to be much smaller. Considering also the different weight factors for Ti and O_p atoms, it can be inferred that the correlation of the Ti($3sp$) orbitals contributes very little to the total dispersion energy. The fitting of the increments accounting for the helium interaction with the subsurface oxygen atom required an extra R^{-10} term. These increments contribute to less than 4% of the net inter-monomer correlation at the vdW minimum. As can be seen from Table II, the (short-range) three-body He–O_p–O_p increments contribute very little (6% of the two-body counterpart), showing the effective pairwise behavior of the dispersion interactions.

Focusing now on the intra-monomer correlation terms (see Table II), we have found an exponential decay of the one- and two-body repulsive increment contributions as a function of the He–Ti(5f) distance. As shown in Fig. 3, we have identified these terms with the correlation contribution to the exchange-repulsion energy component. The enhanced exchange-repulsion when the correlation is accounted for has been interpreted in terms of the effect called "truncation of the correlation space" by Staemmler.[50,92] Indeed, a number of virtual excitations experienced by the electrons of one monomer to avoid each other becomes blocked when some orbitals are occupied by the electrons of the other monomer. It is thus strongly influenced by the energy location and shape of the "blocking" monomer occupied orbital (*e.g.*, the He($1s$) orbital) and also the energy gap to the virtual orbitals. This repulsive contribution is added to the repulsion LMO-EDA energy component from the Hartree-Fock wave-function, reflecting the enhanced inter-electronic Coulomb repulsion within each monomer upon the orthogonalization of the HF occupied orbitals to those of the other monomer. As a short-range correlation contribution, the magnitude of the exchange-repulsion-like term increases steeply as the inter-monomer distance decreases. For example, it amounts to 21% and 38% of the total correlation energy at $z = 3.875$ and 3.5 Å, respectively.

At this point, we would like to stress two aspects. First, it is not possible to rigorously

map SAPT-based energy components to the correlation contributions from supermolecular post-HF calculations. Therefore, the performance of SAPT(DFT) approaches is usually tested through the comparison with total CCSD(T) interaction energies. Aimed to fill this gap, the SAPT(CCSD) method has been recently developed by Korona (see, *e.g.*, Ref. 93 and references cited therein). In this work, the incremental partitioning of the CCSD(T) correlation has been applied along with the LMO-EDA of the HF interaction energy to perform the mapping between SAPT(DFT) energy components and CCSD(T) correlation contributions. For very weakly interacting systems composed by neutral closed-shell monomers, intra- and inter-monomer correlation contributions can be well identified with the correlation contribution to the exchange-repulsion/dispersion energy components. The excellent agreement between CCSD(T) and SAPT(PBE0) individual components confirms the reliability of this mapping. Second, the LMO-EDA scheme of Su and Li[20] identifies the whole CCSD(T) correlation contribution with the dispersion energy component instead of being separated as in our case. Similarly, the DFT correlation energy (E_c) modification when going from the separated monomers to the complex is entirely accounted for within the inter-monomer LMO-EDA correlation energy component $\mathrm{E}_{corr}^{\mathrm{inter}}$ (see Eq. 9), being identified with the short-range dispersion. Our results suggest that the changes in E_c could be also taken into account within the exchange-repulsion energy term, in an analogous way to the DFT exchange energy contribution to the repulsion term (see Eq. 8).

C. Assessing the accuracy of the dlDF and SAPT(DFT) methods: He–$(TiO_2)(H_2O)_3$ interaction energies and nuclear bound states

To assess the accuracy of the dlDF and SAPT(DFT) methods, we have performed CCSD(T)-F12b calculations using all-electron augmented triple- and quadruple-ζ orbital basis sets (AVTZ and AVQZ, see Section II), followed by the extrapolation to the CBS limit. For benchmarking purposes, we have also calculated the nuclear bound states supported by the He–$(TiO_2)(H_2O)_3$ potential (see Table III and Figure 5). By comparing the CCSD(T)-F12b/AVTZ and CCSD(T)-F12b/CBS results (see Fig. 2 and Table III), it can be noticed that the interaction energies with the AVTZ basis are not yet converged. The well-depth minimum is ~ 8 cm^{-1} (16.5 %) above the CCSD(T)-F12b/CBS vdW minimum, and the transition energies $\nu_{1\leftarrow 0}$ and $\nu_{2\leftarrow 1}$ between vibrational energy levels are red-shifted

by about 3 cm^{-1} (14–33%) with respect to the benchmark values (see Table III). On a contrary, the CCSD(T)-F12b/AVQZ interaction energies are very close to the estimated CBS limit and the transition energies $\nu_{1\leftarrow 0}$ and $\nu_{2\leftarrow 1}$ are red-shifted by 1.5 cm^{-1} only. The helium nuclear wave-functions are also very close, with the only distinguishable difference being the delocalization degree of the highest-energy bound-state (see Fig. 5). The improvement of coupled-cluster results upon the inclusion of functions explicitly depending on the inter-electronic distance is already a well-known feature (see, *e.g.*, Ref. 84 for an extensive analysis on weakly interacting dimers). In our case (see Fig. 2), this improvement is particularly noticeable at the short-range region while the attractive tail is already well described at CCSD(T)/(A)VTZ level. This can be expected from the better description of the inter-electronic cusp with CCSD(T)-F12 methods, and thus short-range correlation effects as those associated with the exchange-repulsion. An automatic implementation of the incremental CCSD(T)(F12) scheme has been recently reported by Friedrich and collaborators[94] but no applications to transition-metal oxides have been reported yet.

Comparing the SAPT(DFT) and CCSD(T)-F12b potential energy curves (see the upper panel of Figure 4), it can be noticed that the SAPT(DFT) interaction energies using the PBE0 and dlDF functionals closely follow those from the CCSD(T)-F12b method. The SAPT(PBE) approach also provides a very reasonable potential, but clearly too repulsive at short-range, indicating the overestimation of the exchange-repulsion contribution. On a contrary, as shown in the bottom panel of Figure 4, the dispersion energies depend weakly on the density functional used. Still, they are slightly overestimated with the PBE functional so that the potential at the medium-range region is a little bit more attractive than the benchmark. Interestingly, the overestimation of the repulsive (exchange) component is somewhat compensated by that of the attractive (dispersion) contribution so that the nuclear bound-state energies agree to within 2% with those obtained through CCSD(T)-F12b/AVTZ calculations (see Table III). Using the PBE0 functional, both the PEC (see Fig. 4) and the nuclear bound-state energies lay in between the CCSD(T)-F12b counterparts using the AVTZ and AVQZ basis sets. The SAPT(dlDF) approach clearly offers an even better agreement with the benchmark: the interaction energies at the vdW minimum and beyond differ from those obtained through CCSD(T)-F12b/AVQZ calculations by less than 2% while, in the repulsive potential region, they become relatively closer to the estimated CBS limit. This is the reason why the highest-energy nuclear wave-function (see

Fig. 5) is slightly less extended than the CCSD(T)-F12b/AVQZ counterpart. On the other hand, the transition energies $\nu_{1\leftarrow 0}$ and $\nu_{2\leftarrow 1}$ agree to within 0.1% with those calculated at CCSD(T)-F12b/AVQZ level.

Besides testing the performance of SAPT(DFT) approaches through the comparison with CCSD(T) total interaction energies, it is convenient to extend the analysis to the individual energy components. For this purpose, the estimations of the dispersion energies at CCSD(T)/(A)VTZ level, as extracted using the method of increments, are also shown at the bottom panel of Fig. 4. Taking into account the different theoretical grounds of the applied methods, it is worth stressing that the SAPT(DFT) dispersion contributions agree remarkably well with the CCSD(T)/(A)VTZ incremental counterparts (to within 3% for both PBE0 and dlDF functionals). Moreover, the incremental scheme at CCSD(T) level and the SAPT(PBE0) approach provide values for the correlation contribution to the exchange-repulsion in quantitative agreement within 4% (26.92 *vs.* 27.52 cm^{-1} at the vdW minimum). Once again, the SAPT(PBE) approach overestimates the magnitude of this component, with the differences from the corresponding SAPT(PBE0) of about 35%. The exchange-repulsion becomes reduced in SAPT(dlDF) calculations by almost the same percentage. This can be explained considering that the KS orbitals of the monomers are more localized when the dlDF functional is used. As for the intra-monomer correlation contribution to the exchange-repulsion, it affects mostly the potential wall, making it even more repulsive. Our results indicate the overestimation of these contributions when calculated at CCSD(T)/(A)VTZ level. This way, it can be understood why the SAPT(dlDF) potential is closer to the CCSD(T)-F12b/AVQZ potential than the SAPT(PBE0) potential.

Having assessed the accuracy of SAPT(DFT) interaction energies (both total and dispersion and dispersionless energy components), we now evaluate the performance of the dlDF and dlDF+D approaches, with the dispersion contribution (denoted as D) extracted from the SAPT(dlDF) calculations. By subtracting from the benchmark interaction energies, the dispersionless dlDF values, it is clear that we should recover the dispersion component of the interaction as a function of the inter-monomer distance. As clearly apparent from the bottom panel of Fig. 4, this is indeed the case. The dlDF+D potential is in fact very close to the benchmark (see Fig. 2), with the only noticeable difference in the region between the minimum and the long-range tail (the dlDF+D potential is slightly more attractive). The accuracy of the dlDF+D potential can be further assessed by comparing directly the

bound-state energies and wave-functions (see Table III and Fig. 5). The average relative error of the vibrational energies is 3.3% only, with the dlDF+D values being larger. This way, the vibrational states with $v = 1$ and 2 are more localized than the benchmarks (see Fig. 5). Taking into account the approximations used for our benchmark calculations (*e.g.*, the neglect of higher order correlation in the CCSD(T) method and the correlation of the valence electrons only), we can consider that the performance dlDF+D approach on the He–$\mathcal{C}_1$ interaction is very satisfactory.

D. Fitting of the dispersion interaction energies to the D_{as} functional form

To analyze the transferability properties of the dispersion upon augmenting the $\mathcal{C}(TiO_2)$ cluster size, we have fitted the dispersion He–$\mathcal{C}_1$ interaction energies to the effective inter-atomic functional form proposed in Ref. 24 and improved in Ref. 26 (referred to as D_{as}),

$$D_{as} = \sum_{x \in \mathcal{C}_1} -\frac{\sqrt{C_6^{\mathrm{He}} C_6^x}}{R_{\mathrm{He}-x}^6} f_6\left(\sqrt{\beta_{\mathrm{He}}\beta_x} R_{\mathrm{He}-x}\right) - \frac{\sqrt{C_8^{\mathrm{He}} C_8^x}}{R_{\mathrm{He}-x}^8} f_8\left(\sqrt{\beta_{\mathrm{He}}\beta_x} R_{\mathrm{He}-x}\right) \qquad (12)$$

where x numbers the atoms within the cluster $\mathcal{C}_1$ and $f_{6,8}$ are the damping functions of Tang and Toennies[95]. It should be mentioned that the parameters of the D_{as} function were not previously fitted on molecular systems containing the Ti atom. Therefore, we optimized the C_6^{Ti}, C_8^{Ti} and damping β^{Ti} coefficients, freezing the parameters of the other atoms to the original values in Ref. 26. A relative RMS of 1.8% was thus obtained. By performing a global fitting of all the parameters, the relative RMS was slightly lower (1.5%) with the optimized values departing little from those reported in Ref. 26. This indicates an effective atom-in-molecule-like behaviour. We notice, however, that the C_6^x parameters entering into the D_{as} function should not be confused with the C_6 coefficients extracted with the method of increments for the helium interaction with localized orbital groups centered on the O atoms. As already mentioned, the Ti($3d$) atomic orbitals also contribute to these groups due to the partial covalent bonding. In any case, the C_6 coefficients associated to He−O and He−Ti atomic pairs within the D_{as} function are not comparable to those obtained for the ionic He−O^{2-} and He−Ti^{4+} counterparts. Thus, from the $\sqrt{C_6^{\mathrm{He}} C_6^{\mathrm{O}}}$ term in Eq. 12, we obtain a value of 4.07 a.u., which is about three times smaller than that calculated using the Slater-Kirkwood formula (11.47 a.u.).

E. The He–$(TiO_2)_3(H_2O)_5$ complex

Focusing on the next cluster size (the $\mathcal{C}_2$ cluster, see Fig. 1), dispersionless and dispersion-accounting interaction energies of the He–$\mathcal{C}_2$ complex as a function of the He–Ti(5f) distance are plotted in Fig. 6 while the decomposition of the net interaction at the vdW minimum is shown in Fig. 7 (along with the He–$\mathcal{C}_1$ and He–$\mathcal{C}_2$ counterparts). The reference CCSD(T) interaction energies were calculated using a dual basis set: (1) the He atom and the O and Ti atoms in the main interaction region[7] were described with the same basis set as used for the incremental calculations (denoted as (A)VTZ, see above) but supplemented with a hydrogenic aug-cc-pVTZ set of mid-bond functions; (2) the cc-pVDZ basis set of Dunning was employed for the atoms outside the main interaction region.

The first thing to note from Fig. 6 is that both dlDF and SAPT(DFT) approaches provide very similar values for the dispersionless contribution over the whole range of inter-monomer distances. This energy component is rather similar to that obtained for the He–$\mathcal{C}_1$ complex. Still, as can be seen from Fig. 7, the exchange-repulsion is somewhat smaller. As compared with the $\mathcal{C}_1$ counterpart, the $\mathcal{C}_2$ cluster partially accounts for the extended nature of the surface along the Ti(5f) atom row. The additional oxygen atoms are rather far away from the helium atoms so that the enhancement of the net dispersion term is rather modest (about 15% at most). The decreased exchange-repulsion and the intensified dispersion-attraction come together to make the potential well about 20 cm^{-1} deeper (see Fig. 6).

It is also worth stressing that the differences on the dispersionless SAPT(DFT) energies depending on the functional adopted are smoothed out when the cluster is enlarged. This is even more clear in Fig. 8, where the dispersionless contribution to the total interaction energy has been plotted for each cluster size. By comparing SAPT(ALDA/dlDF) and SAPT(PBE) interaction energies, we can notice that the dispersion component of the interaction is apparently influenced by the chosen functional. However, as discussed in Ref. 36, this is a consequence of using a pure ALDA kernel in calculations with non-local xc potentials when the density-fitting approximation is used. The results obtained for the He–$\mathcal{C}_1$ complex show that the dispersion energy is underestimated by about 7.5% (17%) when the ALDA/PBE0 (ALDA/dlDF) kernel is used instead of an hybrid xc kernel with 25% (61.44%) of single-determinant exchange. Accordingly, SAPT(ALDA/dlDF) and SAPT(ALDA/PBE0) interaction energies become very close to those calculated with the SAPT(PBE) approach when

their respective dispersion components are augmented by 17% and 7.5%, respectively.

As can be seen in Fig. 6, the SAPT(ALDA/PBE0) potential is almost indistinguishable from that obtained through CCSD(T) calculations. The small underestimation of the dispersion energy with the SAPT(ALDA/PBE0) model is thus compensated by the basis set incompleteness in our benchmark CCSD(T) calculations for the He–$\mathcal{C}_2$ complex. We have tested that the CCSD(T) well-depth with the same basis differs by about 12% from the CBS estimate for the He–$\mathcal{C}_1$ system. The SAPT(DFT) interaction energies are better converged with respect to the orbital basis set size so that additional diffuse functions causes a shift of the dispersion component by $\sim 4\%$ only (see Section II). An overall very good agreement between SAPT(PBE0) and CCSD(T) interaction energies of weakly bound systems has been pointed out by Jansen and collaborators (see, for example, Ref. 96). Considering the basis set incompleteness in our CCSD(T) calculations, it seems that the SAPT(PBE) approach performs also rather well for the He–$\mathcal{C}_2$ complex.

Considering the interaction energies calculated with the dlDF+D and dlDF+D_{as} approaches (see Fig. 6), it can be noticed that SAPT(PBE) and dlDF+D_{as} PECs are almost identical to each other, differing also very little from the dlDF+D curve. Hence, it turns out that the dlDF+D_{as} approach is also an excellent performer for the He–$\mathcal{C}_2$ system. Moreover, the similarities between the dispersion energies fitted from the He–$\mathcal{C}_1$ complex, and calculated directly for the He–$\mathcal{C}_2$ complex (and also the He–$\mathcal{C}_3$ system, as discussed below), indicate that this energy component is effectively pairwise additive, and highly transferable from one cluster size modeling the extended system to another. We also mention that the D_{as} dispersion energies with the parameters obtained through the global fitting differed very little from those calculated with the constrained fitting (i.e., optimizing the Ti parameters only).

F. The He-$(TiO_2)_9(H_2O)_7$ complex: correlation effects

As can be seen in Fig. 1, the largest cluster model of the rutile surface (the $\mathcal{C}_3$ cluster with stoichiometry $(TiO_2)_9(H_2O)_7$) already includes the bridging oxygen atom O_b rows. The key role of the O_b rows has been highlighted in previous physisorption studies on the same surface.[7,57] As will be shown, the subdivision of the net interaction energy provides further insights into the reasons of this behavior. Figure 7 illustrates how the individual energy

components of the interaction are being modified upon expanding the cluster size from $\mathcal{C}_1$ to $\mathcal{C}_3$, as evaluated with the SAPT(PBE0) approach. They are calculated at an intermediate He–Ti(5f) distance between the vdW minima of the He–$\mathcal{C}_{1,2}$ and He–$\mathcal{C}_3$ dimers ($z = 3.25$ Å). As can be seen in Fig. 7, the He-cluster interaction becomes a factor of 4 more attractive upon expanding the cluster model from $\mathcal{C}_1$ to $\mathcal{C}_3$. The most obvious reason is the inclusion of the dispersion He–O_b interaction with the $\mathcal{C}_3$ cluster. In the vdW minimum region, the distance separating the helium atom and the two nearest bridging oxygen atoms O_b differs very little from the He–O_p distance (*e.g.*, by 0.15 Å at $z = 3.25$ Å). As mentioned above (see Table II), the two-body He–O_p increments contribute to more than 90% of the net dispersion He–$\mathcal{C}_1$ interaction energy. Considering the effectively pairwise additive character of the dispersion He–$\mathcal{C}_2$ interaction, it can be expected that the two adjacent O_b atoms in $\mathcal{C}_3$ enhance the net dispersion contribution by a factor of ~ 1.5. As can be observed from Fig. 7, this is certainly the case: the dispersion energy increases from -150 cm^{-1} in $\mathcal{C}_1$ to about -220 cm^{-1} in $\mathcal{C}_3$. From Fig. 7, it can be also noticed that the induction interaction is more attractive (by about 22 cm^{-1}) when atoms from internal molecular layers are included with the $\mathcal{C}_3$ cluster model of the rutile surface. On a contrary, the induction component changes very little when the $\mathcal{C}_1$ cluster is extended along the parallel direction to the surface with the $\mathcal{C}_2$ cluster model. Nonetheless it is very important to notice that these are not the only factors in making the whole interaction more attractive: the He–$\mathcal{C}_1$ exchange-repulsion is reduced by about 30% (~ 50 cm^{-1}) for the He–$\mathcal{C}_3$ complex. This is somewhat surprising, assuming that effective pairwise He–O_b Pauli repulsive interactions are added to those of the He–O_p pairs. The electronic density around the O_p atoms, however, differs considerably in $\mathcal{C}_1$ and $\mathcal{C}_2$ clusters. As pointed out by Rittner et al.,[57] the O_p atoms become squeezed out when bounded to Ti atoms within the $\mathcal{C}_3$ cluster (i.e., instead of the hydrogen atoms saturating the $\mathcal{C}_1$ counterpart). This compression of the electronic density is reflected in the reduction of the electrostatic attraction by a factor of 1.6 (see Fig. 7). This explains why the uncorrelated HF exchange-repulsion decreases by 20 cm^{-1} when going from $\mathcal{C}_1$ to $\mathcal{C}_3$. Since the exchange-repulsion energy is further overshooted, it is obvious that there is also a correlation effect at play in reducing this contribution. As clearly apparent from Fig. 9, both the decreased exchange-repulsion and the increased induction concur in providing dispersionless He–$\mathcal{C}_3$ interaction energies rather below the He–$\mathcal{C}_1$ counterparts, over the whole range of inter-monomer distances.

In order to get insights into the main correlation effect responsible for the reduction in the exchange-repulsion, the method of increments has been applied to the He–$\mathcal{C}_3$ complex with the MP2, LMP2, LCCSD(T) and CCSD(T) methods using the (A)VDZ basis (see Section II for the computational details). The most important incremental contributions are collected along with the He–$\mathcal{C}_1$ counterparts in Table IV. The values obtained for the He–$\mathcal{C}_1$ complex with the (A)VTZ basis are also tabulated. From the comparison to the results with the (A)VTZ basis, we can notice that the dispersion CCSD(T) He–O_p term is underestimated by about 13% using the (A)VDZ basis, with the dispersionless contributions lying to within 16% the (A)VTZ counterpart. Focusing on the incremental contributions obtained with the CCSD(T) approach (shown in boldface), it can be noticed that the correlation contribution to the He–$\mathcal{C}_3$ interaction energy E_{int}^{corr} is a factor of 1.7 larger than the E_{int}^{corr} value obtained for He–$\mathcal{C}_1$ dimer and the same basis. In agreement with the analysis of SAPT(DFT) energy components, only part of this increased correlation can be attributed to the additional attractive He–O_b interactions in the He–$\mathcal{C}_3$ system: it turns out that the dominant (repulsive) one-body incremental contribution is more than doubled in the $\mathcal{C}_1$ dimer. In both cases, this correlation term is dominated by the one-body $\eta(O_p)$ increment modification when going from the bare $\mathcal{C}_x$ ($x = 1, 2$) cluster to the He–$\mathcal{C}_x$ dimer. Once again, this is the main correlation contribution to the exchange-repulsion. Albeit its magnitude raises as the inter-monomer He–$\mathcal{C}_3$ distance decreases, it stays well below the He–$\mathcal{C}_1$ counterpart. As mentioned above, this exchange-repulsion-like contribution can be rationalized in terms of the correlation space truncation of the electrons from the O_p atoms by the He($1s$) orbital. It is influenced by both the energy and shape of the He($1s$) orbital with respect to the valence O_p($2s$,$2p$) orbitals and the energy gap to the low-lying virtual orbitals. At HF level, the energy of the border HOMO orbital (mostly formed by the O_p($2p$) atomic orbital) varies very little from the $\mathcal{C}_1$ to the $\mathcal{C}_3$ cluster. On a contrary, the HOMO-LUMO gap in $\mathcal{C}_3$ is almost half of the value in $\mathcal{C}_1$. As in Ref. 46, the appearance of lower-lying excitations can be explained by the better description of the O_p diffuse tail when the electrons are allowed to flow to the neighbor titanium atoms in the $\mathcal{C}_3$ cluster. On the other hand, the energy of the orbital oriented in the O_p–H direction in $\mathcal{C}_1$ is very close to that of the He($1s$) orbital, thus enhancing the correlation space truncation effect. The energy and space location of the O_b($2p$) orbitals make them less affected, despite the very similar He–O_p and He–O_b distances. As a result, the $\eta(O_b)$ increment contribution is a factor of 10 smaller

than the $\eta(O_p)$ counterpart (see Table IV). For ionic materials such as the MgO(100) surface, the electronic charges are more confined and therefore the exchange-repulsion term is less influenced by the cluster model (see, for example, Ref. 38). As a partially covalent material, the realistic *ab initio* estimation of the intra-monomer correlation contribution to the interaction energy, neccesitates the inclusion of the main interacting atoms from the rutile surface along with their first coordination shells within the cluster model. This is in contrast to the inter-monomer correlation contribution (i.e., the dispersion): as clearly shown in Table IV, the two-body He–O_p dispersion interaction changes very little (5% at worst) when going from $\mathcal{C}_1$ to the $\mathcal{C}_3$ cluster for all the methods considered. This finding is further confirmed by the comparison between the dlDF+D and dlDF+D_{as} He–$\mathcal{C}_3$ PECs shown in Fig. 9: the dispersion energies calculated directly for the He–$\mathcal{C}_3$ complex match almost perfectly those fitted from the He–$\mathcal{C}_1$ interaction.

The CCSD(T) results reported in Table IV can be also compared with those obtained with the MP2, LMP2 and LCCSD(T) approaches. The first thing to observe is that all these approaches significantly underestimate the correlation contribution to the interaction energy. At MP2 level of theory, both the overestimated repulsive intra-monomer correlation terms and the underestimated attractive He–O inter-monomer increments are responsible for such behavior. On the other hand, from the comparison of the most important LCCSD(T) and CCSD(T) incremental contributions as well as the LMP2 and MP2 counterparts, the tendency of the local correlation treatment to further reduce the dispersion terms is clearly apparent. It should be stressed, however, that `MOLPRO` default parameters were employed within the LMP2 and LCCSD(T) frameworks so that their optimization should provide results closer to the MP2 and CCSD(T) counterparts.

G. The He-$(TiO_2)_9(H_2O)_7$ complex: potential energy curves

Let us now compare the PECs shown in Fig. 9, as obtained from supermolecular and SAPT-based calculations. We have calculated a reference value of the He–$\mathcal{C}_3$ interaction energy at LCCSD(T) level of theory, using the ext-TVAE** basis set and choosing a geometry at the minimum region (z = 3.75 Å, see Fig. 9). The interaction becomes more attractive by about 22% at LCCSD(T) level (-108.2 cm^{-1}) as compared with the LMP2 counterpart (-84.7 cm^{-1}). A similar enhancement (about 25%) is found for the main correlation part

of the interaction energy when it is treated at CCSD(T) level of theory instead of MP2 (see Table IV). The inclusion of the Grimme's spin correction in MP2 makes the interaction even less attractive (by about 20%). Previous studies of the He−MgO(100) extended system with the CRYSCOR code have already pointed out the underestimation of the dispersion contribution at LMP2 level of theory[97].

Similar to the He–$\mathcal{C}_1$ system, it is evident from Fig. 8 that the SAPT(PBE) approach provides a too repulsive dispersionless interaction for the He–$\mathcal{C}_3$ complex. As occurred when the $\mathcal{C}_1$ cluster was expanded along the Ti(5f) rows to build the $\mathcal{C}_2$ model (i.e., the crystallographic [001] direction), it can be expected that a further extension of the $\mathcal{C}_3$ cluster along the crystallographic [$\bar{1}$00] direction weakens down the differences between the SAPT(DFT) estimations for the net dispersionless term, and then the whole interaction energy. Interestingly, the overestimation of the dispersionless He–$\mathcal{C}_3$ interaction energy with the SAPT(PBE) approach is of very similar magnitude to the underestimation of the dispersion term by the SAPT(ALDA/PBE0) and SAPT(ALDA/dlDF) variants. Thus, the differences between the SAPT(PBE) and SAPT(ALDA/PBE0) PECs are almost indistinguishable (see Fig. 9). To avoid the dispersion energy underestimation in the SAPT(ALDA/PBE0) approach, Jansen and collaborators (see, *e.g*, Ref. 36) have proposed a modified version that uses the Localized-Hartree-Fock method. Based on the very weak influence of the chosen functional for the dispersion He–$\mathcal{C}_1$ energies (see the bottom panel of Fig. 4), we have opted for a simpler solution: the dispersion energies calculated at SAPT(PBE) level (denoted as D) have been added to the dispersionless energies evaluated with the SAPT(PBE0) approach. The PEC resulting from this scheme (referred to as SAPT(PBE0)+D) is also plotted in Fig. 9. The interaction energy at z = 3.75 Å (−109.8 cm^{-1}) agrees well with the value obtained at LCCSD(T)/ext-TVAE** level (−108.2 cm^{-1}), considering the approximations involved. The E_{int} value at z = 3.25 Å (−171.8 cm^{-1}) is also consistent with the estimated interaction energy at CCSD(T)/(A)VDZ level (−147.5 cm^{-1}), taking into account the different basis sets. Thus, when the He–O_p increment using the (A)VDZ basis is upscaled by a factor of $\sim$ 1.2, accounting for the difference with that calculated for the He–$\mathcal{C}_1$ complex using the (A)VTZ basis (see Table IV), the estimated E_{int} value becomes lowered to −170.4 cm^{-1}. Finally, the excellent agreement between dlDF+D_{as} and SAPT(PBE0)+D potential energy curves is worth mentioning. Similarly to the He–C_1 and He–C_2 complexes, the dlDF+D_{as} approach has remarkably provided interaction He–C_3 energies lying closer to the expected

"exact" values than those calculated at higher levels of *ab initio* theory.

IV. CONCLUDING REMARKS AND FUTURE PROSPECTS

The benchmark results presented in this contribution clearly show that the SAPT(DFT)[31,32] and dlDF+D[24] methods perform very well in the ultimate dispersion-dominated physisorption problem, involving the helium interaction with clusters modeling a prototype transition-metal-oxide surface.

Using the smallest cluster and the localized molecular orbital energy decomposition (LMO-EDA),[20] we have analyzed the reasons why the most common DFT approach to determine He-surface potentials (the PBE functional) works reasonably well without dispersion corrections and, consequently, poorly in DFT+D constructions. The application of the method of increments[45] to extract the intra- and inter-monomer correlation contributions along with the LMO-EDA partitioning of the HF interaction energy, has allowed us to estimate the individual energy terms characterizing the He-cluster interaction at CCSD(T) level of theory, comparing them with SAPT(DFT)-based components using different DFT functionals (PBE, dlDF, and PBE0). To refine our benchmarks, we have calculated the nuclear bound-state energies and wave-functions supported the He-cluster interaction potentials at CCSD(T)-F12b level of theory, including an estimation of the CBS limit. Although the three considered SAPT(DFT) versions provide results (i.e., bound-state energies) in quantitative agreement with the CCSD(T)-F12b counterparts, the individual dispersionless energy components calculated with the SAPT(DFT) method using the hybrid PBE0 functional are closer to those estimated at CCSD(T) level of theory by means of the method of increments. A similar conclusion has been reached in a systematic analysis using the SAPT(CCSD) method.[93] The hybrid meta functional dlDF, however, provides total interaction energies in better agreement with those obtained at CCSD(T)-F12b level using the largest basis set. The PBE functional within SAPT(DFT) overestimates the exchange-repulsion energy component, giving rise to the least attractive interaction. On a contrary, the dispersion energies calculated with the three SAPT(DFT) approaches agree remarkably well to each other and to those extracted with the incremental scheme at CCSD(T) level. Interestingly, the supermolecular dlDF+D approach has the best agreement with our best benchmark. For instance, the transition vibrational energies differ by less than 0.2% from those obtained

at CCSD(T)-F12b level.

Naturally, whatever the cluster modeling the rutile surface is, the dispersion dominates the attractive interaction. Both SAPT(DFT) and wave-function post-HF (CCSD(T), LCCSD(T), MP2, and LMP2) methods applied within the incremental scheme, demonstrate the high transferability character of the effective pairwise dispersion interaction in extending the cluster model along the different crystallographic directions. This has been made clear by the similarity between the dispersion energies estimated from the fitting of the SAPT(DFT) results for the smallest cluster (referred to as D_{as}), and directly calculated at largest cluster sizes (denoted as D). It has been further demonstrated through the explicit calculation of the dominant inter-monomer increments, characterizing the dispersion interaction, for both the smallest and the largest cluster: they differ by 5% at worst. On a contrary, the short-range intra-monomer correlation (associated to the exchange-repulsion) is not transferable between the two cluster models. For the smallest cluster, it is by far the most difficult correlation effect to deal with and its accurate estimation neccesitates explicitly correlated methods. Fortunately, this contribution is much less important when the extended surface is better modeled. When going from the smallest to the largest cluster, the reduction in the exchange-repulsion is as important as the increase of the dispersion interaction in making the potential well a factor of four deeper. The He–cluster induction interaction becomes significantly more attractive when adding atoms from the internal molecular layers of the rutile surface with the largest cluster model. Contrarily, the extension of the cluster model only along a direction parallel to the surface leaves the inductive component almost unchanged, as the net dispersionless interaction. Therefore, further improvement of the He–TiO_2(110) interaction energies at CCSD(T) level with the incremental scheme would require periodic HF calculations using slab models, enabling a more precise estimation of the long-range inductive term. Similarly, the more accurate determination of the He–TiO_2(110) potential energy surface with the dlDF+D_{as} scheme requires further calculations including periodic boundary conditions. One possible route is to perform periodic dlDF calculations directly and the other possibility is to estimate the intramonomer correlation contribution from dlDF calculations using cluster sizes large enough to ensure its convergence.

The results presented in this contribution have also clearly demonstrated the capability of the method of increments to achieve the accuracy of the CCSD(T) calculations using large cluster models of the TiO_2(110) surface. Moreover, we have illustrated how the combination

of this method with an energy partitioning of the HF interaction energy (as the LMO-EDA scheme) enables to estimate interaction energy components, which can be used as reference values in the design of ad-hoc DFT-based treatments. In this regard, the excellent performance of the dlDF approach (optimized to give the dispersionless component only) is particularly reassuring. Work along these lines is currently in progress.

In concluding, through the application of SAPT(DFT), the method of increments and explicitly correlated CCSD(T) on the helium interaction with cluster models of the rutile surface, we have unambiguously demonstrated both the accuracy of the dlDF+D approach and the high transferability of the effective pairwise dispersion interactions between the different clusters. As a result, an even simpler dlDF+D_{as} scheme, in which the D_{as} dispersion function parameters are fitted using the smallest cluster model, is very reliable. Both the simplicity and accuracy of the dlDF+D_{as} scheme hold promises for the practical determinations of He-surface potential energy surfaces. Extensions to periodic boundary conditions are underway. Likewise, work is currently ongoing to extend the strategy described in this contribution to assess the performance of the dlDF+D_{as} approach on other substrates including graphite and metals, as well as different adsorbates for which the dispersion might be relevant but not necessarily dominant. In this regard, it is worth recalling that Pernal et al.[24] have demonstrated that the dlDF functional works also very well on molecular systems with attractive interactions well beyond the van der Waals regime. As in the present contribution, we expect that these efforts serve to illustrate how the combined DFT and post-HF perspectives may be effective to tailor simple and reliable *ab initio*-driven schemes in surface science applications.

Acknowledgments

It is a pleasure to dedicate this paper to Franco A. Gianturco on the occasion of his 70th birthday. We thank Krzysztof Szalewicz for stimulating discussions and useful suggestions, J. Grant Hill for providing us with auxiliary basis sets prior to publication in Ref. 81, and Georg Jansen for clarifying aspects of the DFT-SAPT implementation. We also thank Néstor F. Aguirre for his contribution in the earliest stage of this work. This work has been performed under Grants Nos. CCG08-CSIC/ESP-3680 from CSIC-CM, and FIS2011-29596-C02-01 from DGI, Spain (FEDER). The support of COST Action CM1002 (CoDECS) is also

gratefully acknowledged. The calculations were performed at the Cesga Super-Computer Center (Galicia) and the Computer Centers at the IFF (CSIC) and the Centro Técnico de Informática (CTI, CSIC).

[1] Farias, D., and Rieder, K. H. (1998) The Transition of Chemisorbed Hydrogen into Subsurface Sites on Pd(311). *Rep. Prog. Phys. 61*, 1575–1664.

[2] Loginov, E., Gómez, L. F., and Vilesov, A. F. (2011) Surface Deposition and Imaging of Large Ag Clusters formed in He Droplets. *J. Phys. Chem. A 115*, 7199–7204.

[3] Aguirre, N. F., Mateo, D., Mitrushchenkov, A. O., Pi, M., and de Lara-Castells, M. P. (2012) Helium-mediated deposition: Moleling the He-TiO_2(110)-(1×1) Interaction Potential and Application to the Collision of a Helium Droplet from Density Functional Calculations. *J. Chem. Phys. 136*, 124703.

[4] Diebold, U. (2003) The Surface Science of Titanium Dioxide. *Surf. Sci. Rep. 48*, 53–229.

[5] Thomson, T. L., and Yates, Jr., J. T. (2006) Surface Science Studies of the Photoactivation of TiO_2-new Photochemical Processes. *Chem. Rev. 106*, 4428–4453.

[6] Grätzel, M. (2001) Photoelectrochemical Cells. *Nature 414*, 338–344.

[7] de Lara-Castells, M. P., Aguirre, N. F., and Mitrushchenkov, A. O. (2012) Physisorption of Helium on a TiO_2(110) surface: Periodic and Finite Cluster Approaches. *Chem. Phys. 399*, 272–280.

[8] Dovesi, R., Saunderds, V. R., Roetti, C., Orlando, R., Zicovich-Wilson, C. M., Pascale, F., Doll, K., Harrison, N. M., Civalleri, B., and Bush, I. J. year CRYSTAL09 User's Manual, Universitá Torino, Torino, 2010. http://www.crystal.unito.it.

[9] Kresse, G., and Furthmüller, J. (1996) Efficient Iterative Schemes for Ab Initio Total-Energy Calculations Using a Plane-Wave Basis Set. *Phys. Rev. B 54*, 11169–11186.

[10] Prates Ramalho, J. P., Gomes, J. R. B., and Illas, F. (2013) Accounting for van der Waals Interactions between Adsorbates and Surfaces in Density Functional Theory Based Calculations: Selected Examples. *RSC Adv. 3*, 13085–13100.

[11] Gianturco, F. A., Paesani, F., Laranjeira, M. F., Vassilenko, V., Cunha, M. A., Shashkov, A. G., and Zolotoukhina, A. F. (1998) Computed and Measured Transport Coefficients for CO-He mixtures: Testing a Density Functional Approach. *Mol. Phys. 94*, 605–622.

[12] de Lara, M. P., Villarreal, P., Delgado-Barrio, G., Miret-Artés, S., Buonomo, E., and Gianturco, F. A. (1995) Fragmentation of Ar_3^+ Clusters via Vibrational Predissociation. *Chem. Phys. Lett. 242*, 336–342.

[13] Wu, Q., and Yang, W. T. (2002) Empirical Correction to Density Functional Theory for van der Waals Interactions. *J. Chem. Phys. 116*, 515–524.

[14] Grimme, S. (2006) Semiempirical GGA-type Density Functional Constructed with a Long-Range Dispersion Correction. *J. Comp. Chem. 27*, 1787–1799.

[15] Grimme, S., Antony, J., Ehrlich, S., and Krieg, H. (2010) A Consistent and Accurate Ab Initio Parametrization of Density Functional Dispersion Correction (DFT-D) for the 94 Elements H-Pu. *J. Chem. Phys. 132*, 154104.

[16] Steinmann, S. N., and Corminboeuf, C. (2011) Comprehensive Benchmarking of a Density-Dependent Dispersion Correction. *J. Chem. Theory Comput. 7*, 3567–3577.

[17] Dion, M., Rydberg, H., Schröder, E., Langreth, D. C., and Lundqvist, B. I. (2004) Van der Waals Density functional for General Geometries. *Phys. Rev. Lett. 92*, 246401.

[18] Dappe, Y. J., Ortega, J., and Flores, F. (2010) Weak Chemical Interaction and van der Waals Forces: A Combined Density Functional and Intermolecular Perturbation Theory Application to Graphite and Graphitic Systems. *Lect. Notes Phys. 795*, 45–79.

[19] Silvestrelli, P. L., Ambrosetti, A., Grubisiĉ, S., and Ancilotto, F. (2012) Adsorption of Rare-Gas Atoms on Cu(111) and Pb(111) Surfaces by van der Waals Corrected Density Functional Theory. *Phys. Rev. B 85*, 165405.

[20] Su, P., and Li, H. (2009) Energy Decomposition Analysis of Covalent Bonds and Intermolecular Interactions. *J. Chem. Phys. 131*, 014102.

[21] Wang, F. F., Jenness, G., Al-Saidi, W. A., and Jordan, K. D. (2010) Assessment of the Performance of Common Density Functional Methods for Describing the Interaction Energies of $(H_2O)_6$ Clusters. *J. Chem. Phys. 132*, 134303.

[22] Gianturco, F. A., and de Lara-Castells, M. P. (1996) Stability and Structure of Rare-Gas Ionic Clusters Using Density Functional Methods: a Study of Helium Clusters. *Int. J. Quantum Chem. 60*, 593–608.

[23] Gianturco, F. A., and de Lara-Castells, M. P. (1996) Structure and Anisotropy of Ionic clusters Using Density Functional Theory. *Chem. Phys. 208*, 25–34.

[24] Pernal, K., Podeszwa, R., Patkowski, K., and Szalewicz, K. (2009) Dispersionless Density

Functional Theory. *Phys. Rev. Lett. 103*, 263201.

[25] Podeszwa, R., and Szalewicz, K. (2012) Density Functional Theory Overcomes the Failure of Predicting Intermolecular Interaction Energies. *J. Chem. Phys. 136*, 161102.

[26] Podeszwa, R., Pernal, K., Patkowski, K., and Szalewicz, K. (2010) Extension of the Hartree-Fock Plus Dispersion Method by First-Order Correlation Effects. *J. Phys. Chem. Lett. 1*, 550.

[27] Podeszwa, R., Cencek, W., and Szalewicz, K. (2012) Efficient Calculations of Dispersion Energies for Nanoscale Systems from Coupled Density Response Functions. *J. Chem. Theory Comput. 8*, 1963–1969.

[28] Zhao, Y., Schultz, N. E., and Truhlar, D. G. (2006) Design of Density Functionals by Combining the Method of Constraint Satisfaction with Parametrization for Thermochemistry, Thermochemical Kinetics, and Noncovalent Interactions. *J. Chem. Theory Comput. 2*, 364–382.

[29] Jeziorski, B., Moszynski, R., and Szalewicz, K. (1994) Perturbation Theory Approach to Intermolecular Potential Energy Surfaces of van der Waals Complexes. *Chem. Rev. 94*, 1887–1930.

[30] Szalewicz, K. (2012) Symmetry-Adapted Perturbation Theory of Intermolecular Forces. *WIREs Comput. Mol. Sci. 2*, 254–272.

[31] Hesselmann, A., and Jansen, G. (2003) Intermolecular Dispersion Energies from Time-Dependent Density Functional Theory. *Chem. Phys. Lett. 367*, 778–784.

[32] Misquitta, A. J., Jeziorski, B., and Szalewicz, K. (2003) Dispersion Energy from Density-Functionl Theory Description of Monomers. *Phys. Rev. Lett. 91*, 033201.

[33] Misquitta, A. J., Podeszwa, R., Jeziorski, B., and Szalewicz, K. (2005) Intermolecular Potentials based on Symmetry-Adapted Perturbation Theory with Dispersion Energies from Time-Dependent Density-Functional Calculations. *J. Chem. Phys. 123*, 214103.

[34] H.-J. Werner,, Knowles, P. J., Knizia, G., Manby, F. R., Schütz, M., Celani, P., Korona, T., Lindh, R., Mitrushchenkov, A. O., and Rauhut et al., G. *MOLPRO, version 2012.1, a package of ab initio programs, see http://www.molpro.net*.

[35] Leforestier, C., Tekin, A., Jansen, G., and Herman, M. (2011) First Principles Potential for the Acetylene Dimer and Refinement by Fitting to Experiments. *J. Chem. Phys. 135*, 234306.

[36] Hesselmann, A., Jansen, G., and Schütz, M. (2005) Density-Functional Theory-Symmetry-Adapted Intermolecular Perturbation Theory with Density Fitting: A New Efficient Method

to Study Intermolecular Interaction Energies. *J. Chem. Phys 122*, 014103.

[37] Bukowski, R., Podeszwa, R., and Szalewicz, K. (2006) Density Fitting Methods in Symmetry-Adapted Perturbation Theory Based on Kohn-Sham Description of Monomers. *J. Chem. Theory Comput. 2*, 400–412.

[38] Karalti, O., Alfé, D., Gillan, M. J., and Jordan, K. D. (2012) Adsorption of a Water Molecule on the MgO(100) Surface as Described by Cluster and Slab Models. *Phys. Chem. Chem. Phys. 14*, 7846–7853.

[39] Adler, T. B., Knizia, G., and H.-J. Werner, (2007) A Simple and Efficient CCSD(T)-F12 Approximation. *J. Chem. Phys. 127*, 221106.

[40] Knizia, G., Adler, T. B., and H.-J. Werner, (2009) Simplified CCSD(T)-F12 Methods: Theory and Benchmarks. *J. Chem. Phys. 130*, 054104.

[41] Pisani, C., Schütz, M., Casassa, S., Usvyat, D., Maschio, L., Lorenz, M., and Erba, A. (2012) CRYSCOR: a Program for the Post-Hartree-Fock Treatment of Periodic Systems. *Phys. Chem. Chem. Phys. 14*, 7615.

[42] Martínez-Casado, R., Mallia, G., Usvyat, D., Maschio, L., Casassa, S., Schütz, M., and Harrison, N. M. (2011) Periodic Quantum Mechanical Simulation of the He-MgO(100) Interaction Potential. *J. Chem. Phys. 134*, 014706.

[43] Marsman, M., Grüneis, A., Paier, J., and Kresse, G. (2009) Second-order Moller-Plesset Perturbation Theory Applied to Extended Systems I. Within the Projector-Augmented-Wave Formalism using a Plane Wave Basis Set. *J. Chem. Phys. 130*, 184103.

[44] Grüneis, A., Booth, G., Marsman, M., Spencer, J., Alavi, A., and Kresse, G. (2011) Natural Orbitals for Wave Function Based Correlated Calculations Using a Plane Wave Basis Set. *J. Chem. Theory Comput. 7*, 2780–2785.

[45] Stoll, H. (1992) Correlation-Energy of Diamond. *Phys. Rev. B 46*, 6700–6704.

[46] Rościszewski, K., Doll, K., Paulus, B., Fulde, P., and Stoll, H. (1998) Ground-State Properties of Rutile: Electron-Correlation Effects. *Phys. Rev. B 57*, 14667–14672.

[47] Stoll, H. (1992) On the Correlation-Energy of Graphite. *J. Chem. Phys. 97*, 8449–8454.

[48] Müller, C., and Paulus, B. (2012) Wavefunction-Based Electron Correlation Methods for Solids. *Phys. Chem. Chem. Phys. 14*, 7605–7614.

[49] Müller, C., Herschend, B., Hermansson, K., and Paulus, B. (2008) Application of the Method of Increments to the Adsorption of CO on the CeO_2(110) surface. *J. Chem. Phys. 128*, 214701.

[50] Staemmler, V. (2011) Method of Local Increments for the Calculation of Adsorption Energies of Atoms and Small Molecules on Solid Surfaces II. CO/MgO(001). *J. Phys. Chem. A 115*, 7153–7160.

[51] Voloshina, E., Usvyat, D., Schütz, M., Dedkov, Y., and Paulus, B. (2011) On the Physisorption of Water on Graphene: A CCSD(T) Study. *Phys. Chem. Chem. Phys. 13*, 12041–12047.

[52] Birkenheuer, U., Fulde, P., and Stoll, H. (2006) A Simplified Method for the Computation of Correlation Effects on the Band Structure of Semiconductors. *Theor. Chem. Acc. 116*, 398–403.

[53] Roetti, C., Dovesi, R., von Armin, M., Alsheimer, W., and Birkenheuer, U. year the CRYSTAL-MOLPRO interface, Max-Planck Institut für Physik komplexer Systeme, Dresden, Germany.

[54] de Lara-Castells, M. P., and Mitrushchenkov, A. O. (2011) A Finite Cluster Approach to an Extended Transition Metal Oxide: a Wave-Function-Based Study. *J. Phys. Chem. C 115*, 17540–17557.

[55] Perdew, J. P., Burke, K., and Ernzerhof, M. (1996) Generalized Gradient Approximation Made Simple. *Phys. Rev. Lett. 77*, 3865–3868.

[56] Truhlar, D. G. (1972) Finite Difference Boundary Value Method for Solving One-Dimensional Eigenvalue Equations. *J. Comp. Phys. 10*, 123–132.

[57] Rittner, F., Fink, R., Boddenberg, B., and Staemmler, V. (1998) Adsorption of Nitrogen on Rutile (110): *Ab Initio* Cluster Calculations. *Phys. Rev. B 57*, 4160–4171.

[58] Busayaporn, W., Torrelles, X., Wander, A., Tomić, S., Ernst, A., Montanari, B., Harrison, N. M., Bikondoa, O., Jourmard, I., and Zegenhagen et al., J. (2010) Geometric Structure of $TiO_2(110)(1\times1)$: Confirming Experimental Conclusions. *Phys. Rev. B 81*, 153404.

[59] Boys, S. F., and Bernardi, F. (1970) Calculation of Small Molecular Interactions by Differences of Separate Total Energies. Some Procedures with Reduced Errors. *Mol. Phys. 19*, 553–566.

[60] Paulus, B., and Stoll, H. The Method of Increments − a Wavefunction-Based Correlation Method for Extended Systems. In *Accurate Condensed-Phase Quantum Chemistry*; Manby, F. R., Ed.; CRC Press: New York, 2010.

[61] Paulus, B. (2006) The Method of Increments − A Wavefunction-based Ab Initio Correlation Method for Solids. *Phys. Rep. 428*, 1–52.

[62] Jeziorski, B., Moszyinski, R., Ratkiewicz, A., Rybak, S., Szalewicz, K., and Williams, H. L.

In *Mehods and Techniques in Computational Chemistry; METECC94*; Clementi, E., Ed.; D. Reidel Publishing Company: STEF, Cagliari, 1993; Vol. B, p 79.

[63] Adamo, C., and Barone, V. (1999) Toward Reliable Density Functional Methods Without Adjustable Parameters: The PBE0 Model. *J. Chem. Phys. 110*, 6158–6170.

[64] Grüning, M., Gritsenko, O. V., van Gisbergen, S. V. A., and Baerends, E. J. (2001) Shape Corrections to Exchange-Correlation Potentials by Gradient-Regulated Seamless Connection of Model Potentials for Inner and Outer region. *J. Chem. Phys. 114*, 652–660.

[65] Misquitta, A. J., and Szalewicz, K. (2005) Symmetry-Adapted Perturbation-Theory Calculations of Intermolecular Forces employing Density-Functional Description of Monomers. *J. Chem. Phys. 122*, 214109.

[66] Lias, S. G. year Ionization Energy Evaluation. NIST Chemistry Web-Book, NIST Standard Reference Database No. 69; online: http//webbok.nist.gov.

[67] Borodin, A., and Reichling, M. (2011) Characterizing TiO_2(110) Surface States by their Work Function. *Phys. Chem. Chem. Phys. 13*, 15442–15447.

[68] E. K. U Gross,, Dobson, J. F., and Petersilka, M. (1996) Density Functional Theory of Time-Dependent Phenomena. *Top. Curr. Chem. 181*, 81–172.

[69] Muscat, J. year *The Phase Stability, Surface Structure and Defect Chemistry of Titanium Dioxide from First Principles Techniques*, Ph. D. Thesis. University of Manchester, Manchester, 1999.

[70] Woon, D. E., and Dunning, Jr., T. H. (1994) Gaussian Basis Sets for Use in Correlated Molecular Calculations. Calculation of Static Electrical Response Properties. *J. Chem. Phys. 100*, 2975–2988.

[71] Van Mourik, T., Wilson, A. K., and Dunning, Jr., T. H. (1999) Benchmark Calculations with Correlated Molecular Wavefunctions XIII. Potential Energy Curves for He_2, Ne_2 and Ar_2 Using Correlation Consistent Basis Sets through Augmented Sextuple Zeta. *Mol. Phys. 96*, 529–547.

[72] Polly, R., H.-J. Werner,, Manby, F. R., and Knowles, P. J. (2004) Fast Hartree-Fock Theory Using local Density Fitting Approximations. *Mol. Phys. 102*, 2311–2321.

[73] Weigend, F. (2002) A Fully Direct RI-HF Algorithm: Implementation, Optimised Auxiliary Basis Sets, Demonstration of Accuracy and Efficiency. *Phys. Chem. Chem. Phys. 4*, 4285–4291.

[74] Weigend, F., Köhn, A., and Hättig, C. (2002) Efficient Use of the Correlation Consistent Basis

Sets in Resolution of the Identity MP2 Calculations. *J. Chem. Phys. 116*, 3175–3183.

[75] Peterson, K. A., Adler, T. B., and H.-J. Werner, (2008) Systematically Convergent Basis Sets for Explicitly Correlated Wavefunctions: The Atoms H, He, B-Ne, and Al-Ar. *J. Chem. Phys. 128*, 084102.

[76] Weigend, F. (2008) Hartree-Fock Exchange Fitting Basis Sets for H to Rn. *J. Comput. Chem. 29*, 167–175.

[77] Valeev, E. F. (2004) Improving on the Resolution of the Identity in Linear R12 Ab Initio Theories. *Chem. Phys. Lett. 395*, 190–195.

[78] Yousaf, K. E., and Peterson, K. A. (2008) Optimized Auxiliary Basis Sets for Explicitly Correlated Methods. *J. Chem. Phys. 129*, 184108.

[79] Yousaf, K. E., and Peterson, K. A. (2009) Optimized Complementary Auxiliary Basis Sets for Explicitly Correlated Methods: aug-cc-pVnZ Orbital Basis Sets. *Chem. Phys. Lett. 476*, 303–307.

[80] Hill, J. G., and Peterson, K. A. (2012) Explicitly Correlated Coupled Cluster Calculations for Molecules Containing Group 11 (Cu, Ag, Au) and 12 (Zn, Cd, Hg) Elements: Optimized Complementary Auxiliary Basis Sets for Valence and Core−Valence Basis Sets. *J. Chem. Theory Comput. 8*, 518–526.

[81] Bross, D. H., Hill, J. G., H.-J. Werner,, and Peterson, K. A. (2013) Explicitly Correlated Composite Thermochemistry of Transition Metal Species. *J. Chem. Phys. 139*, 094302.

[82] Hill, J. G., Mitrushchenkov, A. O., and Peterson, K. A. (2013) *Ab Initio* Ro-Vibrational Spectroscopy of the Group 11 Cyanides: CuCN, AgCN, and AuCN. *J. Chem. Phys. 138*, 134314.

[83] Helgaker, T., Klopper, W., Koch, H., and Noga, J. (1997) Basis-Set Convergence of Correlated Calculations on Water. *J. Chem. Phys. 106*, 9639–9646.

[84] Patkowski, K. (2012) On the Accuracy of Explicitly Correlated Coupled-Cluster Interaction Energies − Have Orbital Results been Beaten Yet? *J. Chem. Phys. 137*, 034103.

[85] de Lara-Castells, M. P., Krems, R. V., Buchachenko, A. A., Delgado-Barrio, G., and Villarreal, P. (2001) Complete Basis Set Extrapolation Limit for Electronic Structure Calculations: Energetic and Nonenergetic Properties of HeBr and $HeBr_2$ van der Waals Dimers. *J. Chem. Phys. 115*, 10438–10449.

[86] Hill, J. G., Peterson, K. A., Knizia, G., and H.-J. Werner, (2009) Extrapolating MP2 and

CCSD Explicitly Correlated Correlation Energies to the Complete Basis Set Limit with First and Second Row Correlation Consistent Basis Sets. *J. Chem. Phys. 131*, 194105.

[87] Foster, J. M., and Boys, S. F. (1960) Canonical Configurational Interaction Prodecure. *Rev. Mod. Phys. 32*, 300–302.

[88] Graziano, G., Klimes, J., Fernández-Alonso, F., and Michaelides, A. (2012) Improved Description of Soft Layered Materials with van der Waals Density Functional Theory. *J. Phys.: Condens. Matter 24*, 424216.

[89] J.-P. Piquemal,, Marquez, A., Parisel, O., and Giessner-Pettre, C. (2005) A CSOV Study of the Difference Between HF and DFT Intermolecular Interaction Energy Values: The Importance of the Charge Transfer Contribution. *J. Comp. Chem. 26*, 1052–1062.

[90] Zhang, Y. K., and Yang, W. T. (1998) Comment on *Generalized Gradient Approximation Made Simple. Phys. Rev. Lett. 80*, 890.

[91] Dimitrov, V., and Sakka, S. (1996) Electronic Oxide Polarizability and Optical Basicity of Simple Oxides. I. *J. Appl. Phys. 79*, 1736–1740.

[92] Kestner, N. R., and Sinanoglu, O. (1966) IntermolecularPotentialEnergy Curves: Theory and Calculations on the Helium-Helium Potential. *J. Chem. Phys. 45*, 194–207.

[93] Korona, T. (2013) A Coupled Cluster Treatment of Intramonomer Electron Correlation Within Symmetry-Adapted Perturbation Theory: Benchmark Calculations and a Comparison with a Density-Functional Theory Description. *Mol. Phys. 111*, 3705–3715.

[94] Friedrich, J., and Walczak, K. (2013) Incremental CCSD(T)(F12)|MP2-F12-A Method to Obtain Highly Accurate CCSD(T) Energies for Large Molecules. *J. Chem. Theory Comput. 9*, 408–417.

[95] Tang, K. T., and Toennies, J. P. (1984) An improved Simple-Model for the van der Waals Potential Based on Universal Damping Functions for the Dispersion Coefficients. *J. Chem. Phys. 80*, 3726–3741.

[96] Tekin, A., and Jansen, G. (2007) How Accurate is the Density Functional Theory Combined with Symmetry-Adapted Perturbation Theory Approach for CH-π and π-π Interactions? A Comparison to Supermolecular Calculations for the Acetylene-Benzene Dimer. *Phys. Chem. Chem. Phys. 9*, 1680–1687.

[97] Martínez-Casado, R., Mallia, G., Usvyat, D., Maschio, L., Casassa, S., Schütz, M., and Harrison, N. M. (2011) He-Atom Scattering from MgO(100): Calculating Diffraction Peak Inten-

sities with a Semi Ab-Initio Potential. *Phys. Chem. Chem. Phys. 13*, 14750–14757.

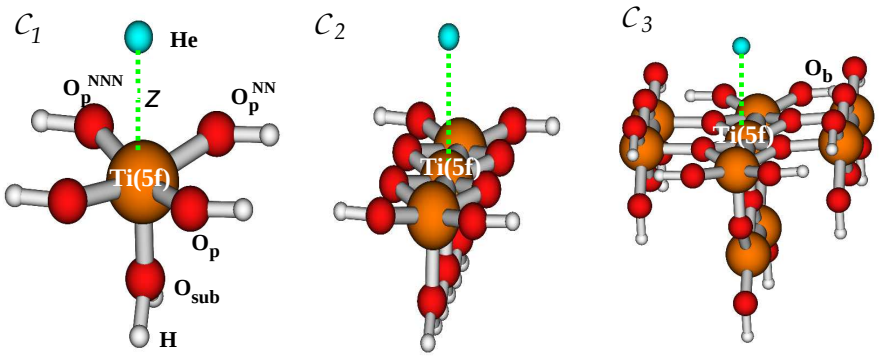

FIG. 1: (color online) Hydrogen-terminated clusters chosen to model the $TiO_2(110)$ surface of stoichiometries $\mathcal{C}_1$: $(TiO_2)(H_2O)_3$, $\mathcal{C}_2$: $(TiO_2)_3(H_2O)_5$, and $\mathcal{C}_3$: $(TiO_2)_9(H_2O)_7$. A reference oxygen (in-plane) surface atom (O_p), the nearest-neighbor (O_p^{NN}) and the next-nearest-neighbor (O_p^{NNN}) are highlighted along with a sub-surface oxygen atom (O_{sub}), the adsorption site (the Ti(5f) cation), and a bridging oxygen atom at the $\mathcal{C}_3$ cluster. The vertical height of a helium atom above the Ti(5f) site (referred to as z) is also indicated.

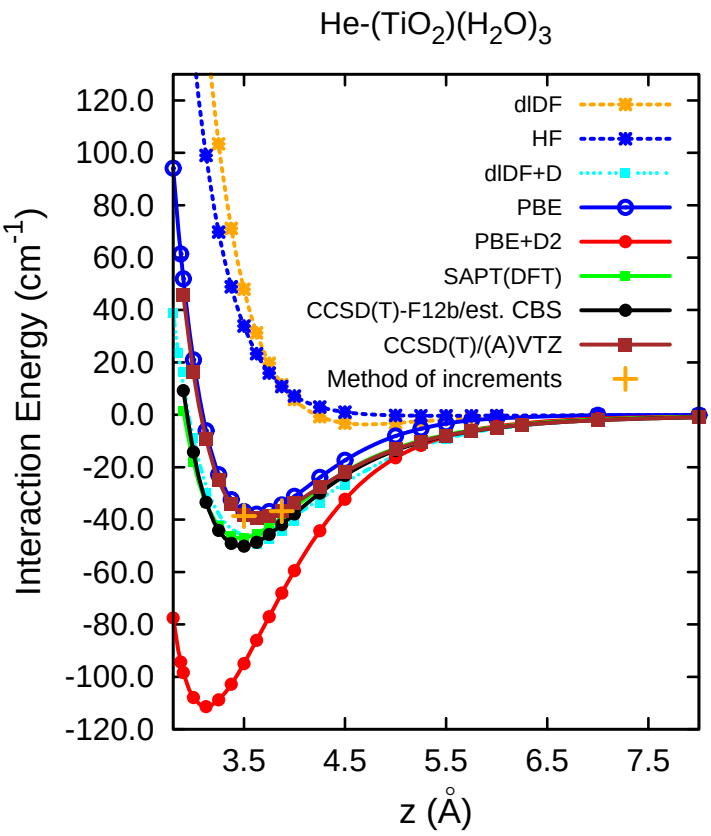

FIG. 2: (color online) He–$\mathcal{C}_1$ interaction energies as a function of the He–Ti(5f) distance (z) using different methodologies (see Fig. 1). The dlDF functional has been used for both the total SAPT(DFT) interaction energies and the dispersion energy component within the dlDF+D construction.

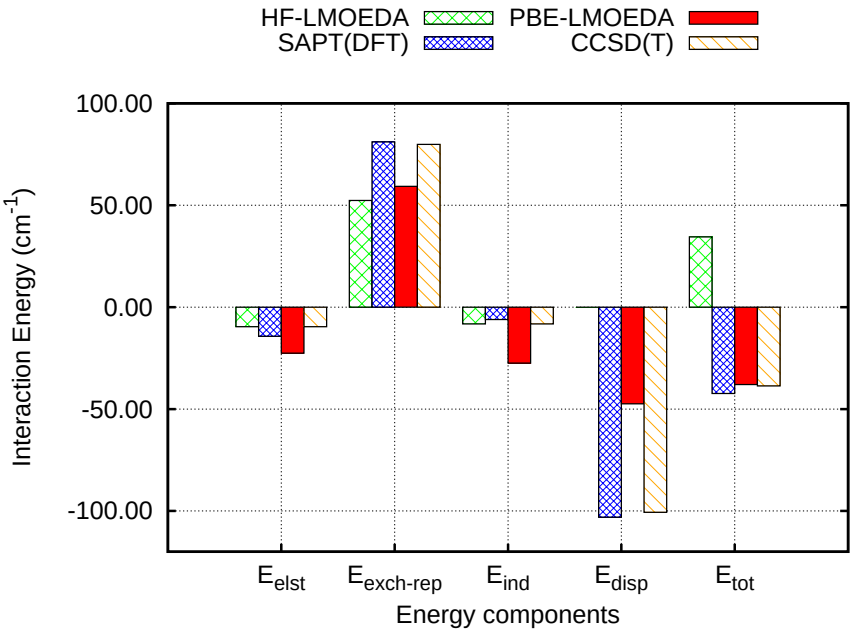

FIG. 3: (color online) Electrostatic, exchange-repulsion, induction, and dispersion contribution to the total interaction energies of the He–$(TiO_2)(H_2O)_3$ complex at the He-Ti distance of $R = 3.5$ Å. The PBE0 functional has been used within the SAPT(DFT) framework. The partitioning of the PBE and HF interaction energies uses the LMO-EDA approach. The CCSD(T) energy components have been obtained by adding the exchange-repulsion and dispersion-like contributions extracted with the method of increments to the HF counterparts (see text).

TABLE I: Minimum energy positions (z_{min}), well-depths (D_e) and zero point energies (ZPE) of the He–$\mathcal{C}_1$ potential energy curves shown in Figs. 2 and 4.

	z_{min}(Å)	D_e(cm^{-1})	ZPE(cm^{-1})
CCSD(T)-F12b: AVTZ/AVQZ/CBS	3.54/3.51/3.48	41.87/46.58/50.14	−26.22/−29.94/−32.80
SAPT(DFT): PBE/PBE0/dlDF	3.67/3.58/3.46	41.07/42.80/46.95	−25.73/−27.25/−30.54
dlDF+D	3.53	50.07	−33.88
PBE	3.61	37.90	−19.68
CCSD(T): (A)VTZ	3.62	39.44	−24.63
PBE+D2	3.13	111.36	−80.68

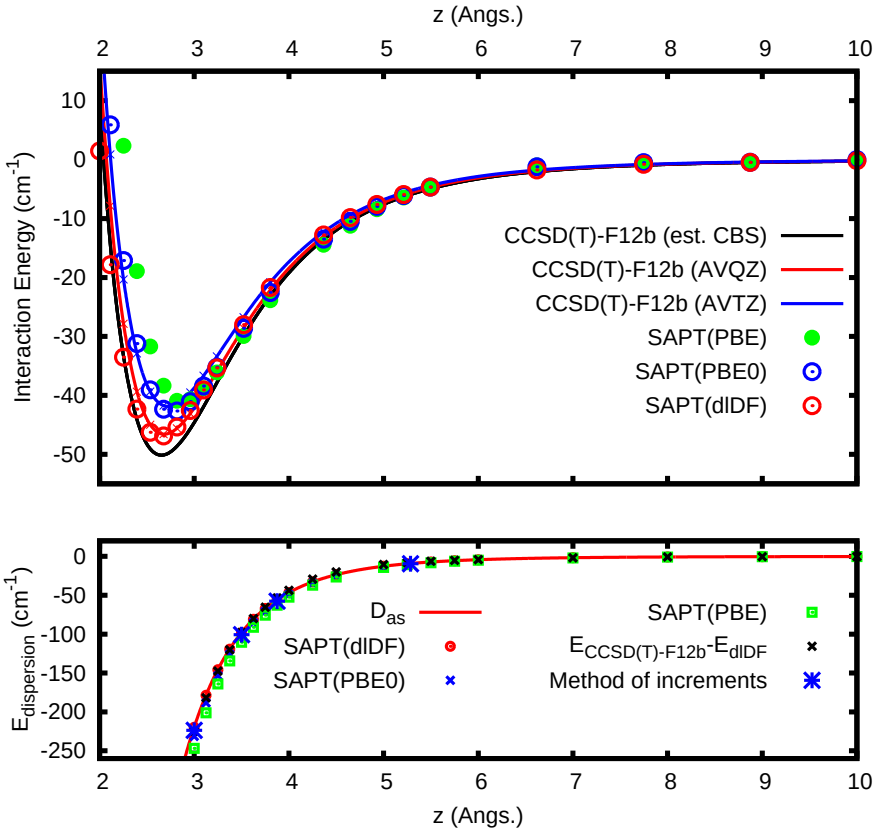

FIG. 4: (color online) Upper panel: Potential energy curves for the He–$\mathcal{C}_1$ complex as obtained with the CCSD(T)-F12b and SAPT(DFT) methods. Bottom panel: Dispersion energies corresponding to the He–$\mathcal{C}_1$ interaction. The dispersion energies obtained with the method of increments include three-body contributions (see text).

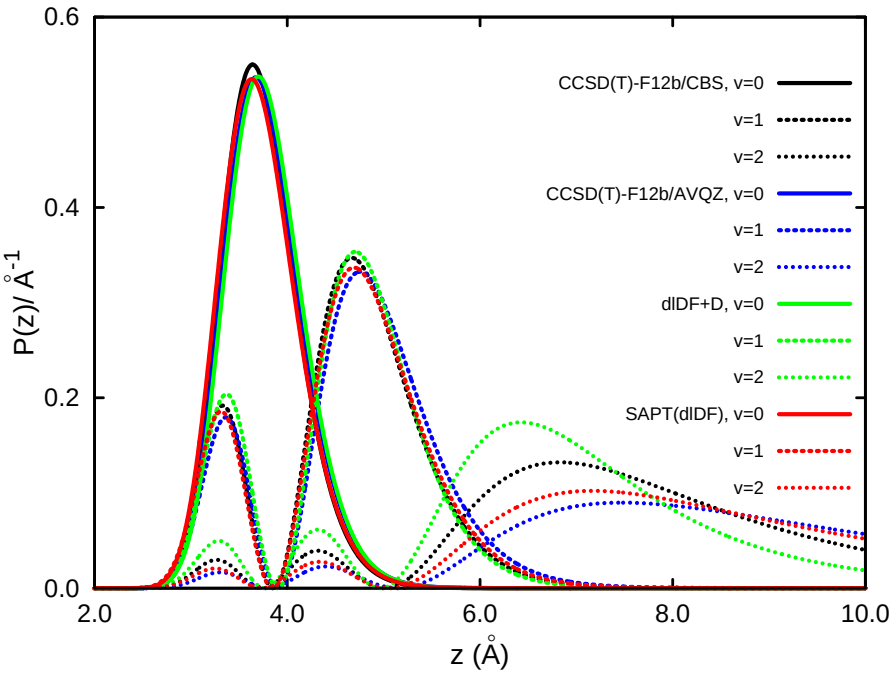

FIG. 5: (color online) Helium probability density distributions of the He–$\mathcal{C}_1$ complex as a function of the He–Ti(5f) distance (see Table III). The distributions are normalized to unity.

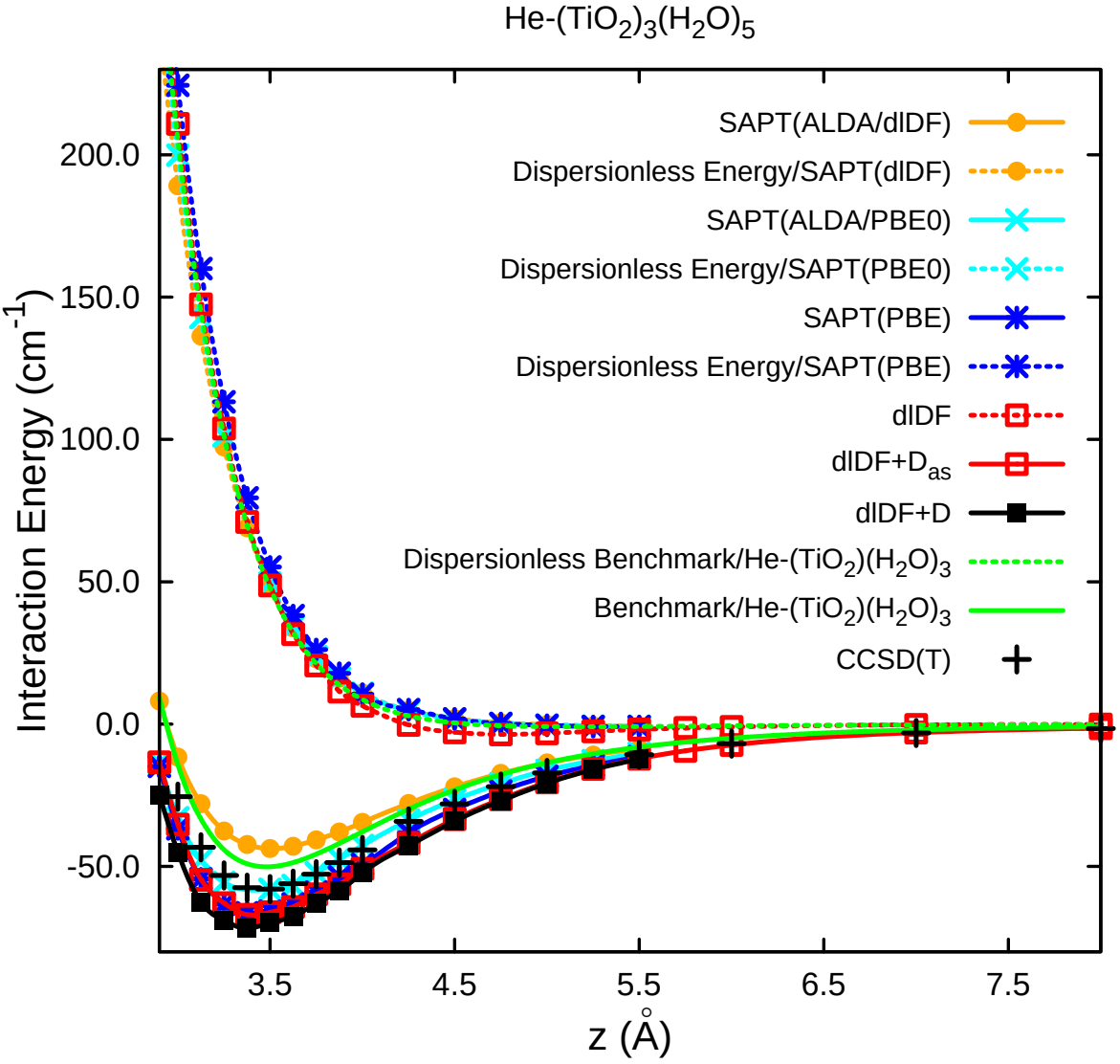

FIG. 6: (color online) Interaction energies of the He–$\mathcal{C}_2$ complex (see Fig. 1) as a function of the He–Ti(5f) distance using different methods. The benchmark for the He–$(TiO_2)(H_2O)_3$ complex corresponds to the CCSD(T)-F12b/CBS total interaction energies. The dispersionless benchmark refers to the difference between CCSD(T)-F12b/CBS total interaction energies and the dispersion energies calculated with the method of increments (see also the bottom panel of Fig. 4). The notation SAPT(ALDA/PBE0) and SAPT(ALDA/dlDF) indicates the use of a pure ALDA kernel in calculating dispersion energies with the hybrid PBE0 and dlDF functionals (see text).

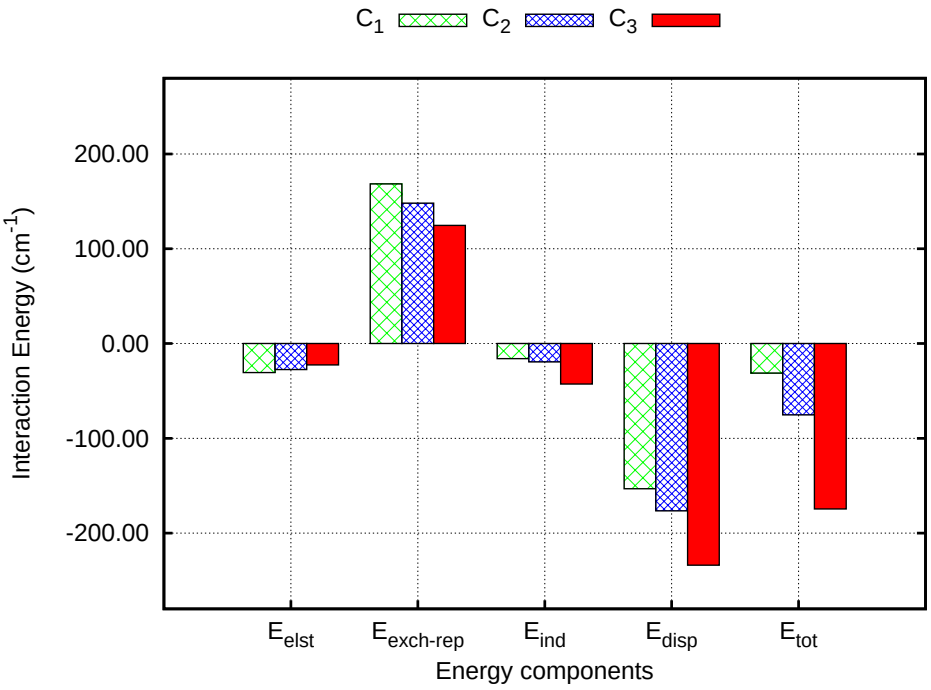

FIG. 7: (color online) Electrostatic, exchange-repulsion, induction, and dispersion contribution to the total interaction energies of the He–$\mathcal{C}_1$, He–$\mathcal{C}_2$, and He–$\mathcal{C}_3$ complexes (see Fig. 1) at the He–Ti(5f) distance of $R = 3.25$ Å. The interaction energy components have been calculated with the SAPT(PBE0) method with the exception of the E_{disp} term in $\mathcal{C}_2$ and $\mathcal{C}_3$, which has been calculated using the PBE functional.

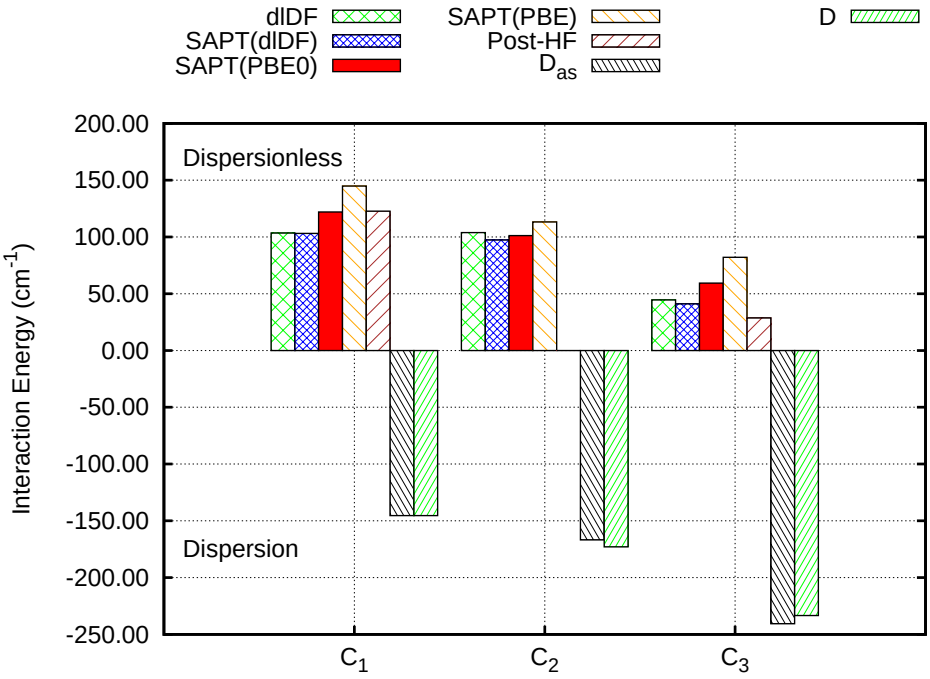

FIG. 8: (color online) Dispersionless contribution to the total interaction energies of the He–$\mathcal{C}_1$, He–$\mathcal{C}_2$, and He–$\mathcal{C}_3$ complexes (see Fig. 1) at the He–Ti(5f) distance of $R = 3.25$ Å, as calculated with the dlDF and SAPT(DFT) approaches. The post-HF values correspond to the sum of the HF interaction energy and the intra-monomer correlation contribution, as extracted with the method of increments at CCSD(T) level of theory using the (A)VTZ and (A)VDZ basis sets for the He–$\mathcal{C}_1$ and He–$\mathcal{C}_3$ complexes, respectively. In the He–$\mathcal{C}_3$ case, only the main incremental contributions to the intra-monomer correlation have been accounted for. For comparison purposes, the dispersion energies fitted from the calculations on the He–$\mathcal{C}_1$ complex (referred to as D_{as}), and directly calculated for the He–$\mathcal{C}_2$ and He–$\mathcal{C}_3$ complexes (denoted as D) are also represented (see text).

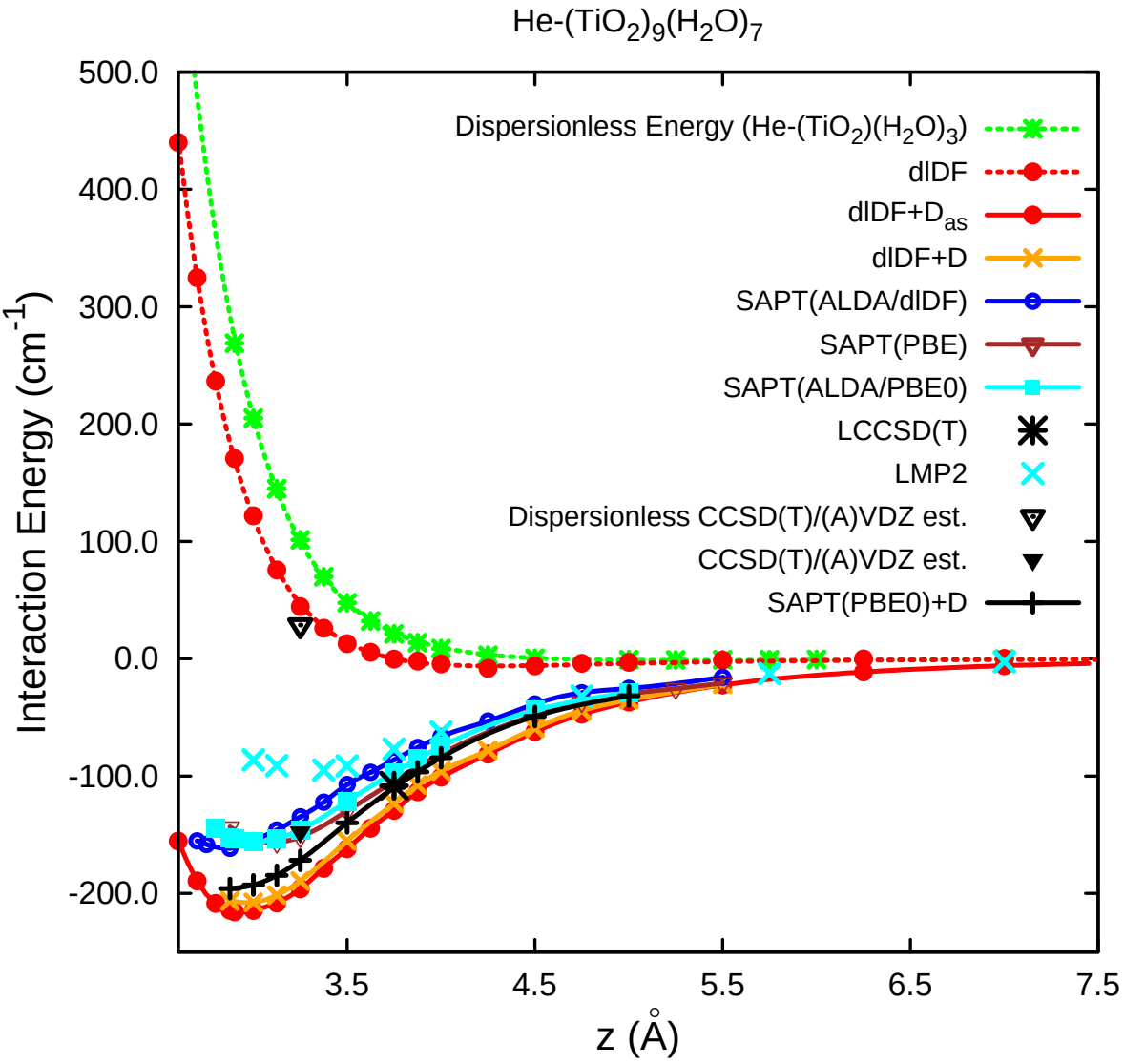

FIG. 9: (color online) Interaction energies of the He–$\mathcal{C}_3$ complex as a function of the He–Ti(5f) distance using different methods (see Fig. 1). The LMP2 interaction energies are those reported in Ref. 7. The dispersionless energy of the He–$(TiO_2)(H_2O)_3$ complex has been calculated as the difference between CCSD(T)-F12b/CBS interaction energies and the dispersion energy components extracted with the method of increments. The SAPT(PBE0)+D notation refers to the sum of dispersionless SAPT(PBE0) interaction energies and dispersion energies calculated with the SAPT(PBE) approach. The CCSD(T) estimations correspond to the sum of the HF interaction energy and the main correlation contributions, as calculated with the method of increments at CCSD(T)/(A)VDZ level of theory (see text).

TABLE II: Selected correlation-energy increment contributions (in cm^{-1}) to the total interaction energy from different orbital groups of the He–$\mathcal{C}_1$ complex at distances of 3.5 and 3.875 Å (see Fig. 1). [b] Correlation contribution to the total interaction energy (E_{int}^{corr}) from full CCSD(T)/(A)VTZ calculations (see text).

Orbital group	Increment contribution	
	$z = 3.5$ Å	$z = 3.875$ Å
One-body contributions		
η(He)	1.7123	0.5779
$\sum_i \eta(O_p^{(i)})$	17.212	5.9600
$\eta(O_{sub})$	−0.0458	−0.0214
Two-body contributions		
$\sum_i \eta(\text{He–}O_p^{(i)})$	−102.806	−58.111
$\eta(\text{He–}O_{sub})$	−3.9367	−2.3257
$\sum_{i<j} \eta(O_p^{(i)}\text{–}O_p^{NN(j)})$	5.2022	1.9073
$\sum_{i<j} \eta(O_p^{(i)}\text{–}O_p^{NNN(j)})$	3.3180	1.5165
$\sum_i \eta(O_p^{(i)}\text{–}O_{sub})$	0.1216	0.0052
Three-body contributions		
$\sum_{i<j} \eta(\text{He–}O_p^{(i)}\text{–}O_p^{NN(j)})$	6.6833	3.5825
$\sum_{i<j} \eta(\text{He–}O_p^{(i)}\text{–}O_p^{NNN(j)})$	−0.5889	−0.6893
E_{int}^{corr}	−73.128	−47.598
	−72.774[b]	−47.316[b]
E_{int}^{HF}	34.482	10.832
E_{int}^{tot}	−38.646	−36.766

TABLE III: Energies of the bound states supported by the He–$\mathcal{C}_1$ potential energy curves shown in Fig. 2 and 4.

	$E_{v=0}(cm^{-1})$	$E_{v=1}(cm^{-1})$	$E_{v=2}(cm^{-1})$
CCSD(T)-F12b: AVTZ/AVQZ/CBS	−26.22/−29.94/−32.80	−6.34/−8.15/−9.60	−0.51/−0.62/−0.86
SAPT(DFT): PBE/PBE0/dlDF	−25.73/−27.25/−30.54	−6.33/−7.11/−8.65	−0.50/−0.50/−0.65
dlDF+D	−33.88	−11.13	−0.91
CCSD(T)/(A)VTZ	−24.63	−5.94	−0.51

TABLE IV: Selected correlation-energy increment contributions (in cm^{-1}) to the total interaction from different orbital groups of the He–$\mathcal{C}_3$ and He–$\mathcal{C}_1$ complexes at the He–Ti(5f) distance of 3.25 Å (see Fig. 1). For the sake of comparison, some increment contributions calculated at CCSD(T)/(A)VTZ level are also tabulated.

Orbital group	$z = 3.25$ Å								
	$\mathcal{C}_3$/(A)VDZ				$\mathcal{C}_1$/(A)VDZ				$\mathcal{C}_1$/(A)VTZ
	MP2	LMP2	LCCSD(T)	CCSD(T)	MP2	LMP2	LCCSD(T)	CCSD(T)	CCSD(T)
One-body									
η(He)	0.51	7.72	5.70	0.73	(2.26)	(4.56)	(5.23)	(3.47)	(3.30)
$\sum_i \eta(O_p^{(i)})$	23.54	22.25	17.77	**17.62**	(47.12)	(45.96)	(37.83)	**(38.99)**	(33.84)
$\sum_i \eta(O_b^{(i)})$	3.80	3.0	1.74	2.19					
Two-body									
$\sum_i \eta(\text{He–}O_p^{(i)})$	−108.84	−99.35	−96.91	**−136.51**	(−103.59)	(−99.10)	(−95.23)	**(−133.12)**	(−153.59)
$\sum_i \eta(\text{He–}O_b^{(i)})$	−35.0	−32.37	−31.57	−39.75					
E_{int}^{corr}	−115.99	−98.75	−103.27	**−155.72**	(−54.22)	(−48.58)	(−52.17)	**(−90.66)**	(−116.45)